REVIEW

Chemically Derived Graphene Oxide: Towards Large-Area Thin-Film Electronics and Optoelectronics

By *Goki Eda* and *Manish Chhowalla**

Chemically derived graphene oxide (GO) possesses a unique set of properties arising from oxygen functional groups that are introduced during chemical exfoliation of graphite. Large-area thin-film deposition of GO, enabled by its solubility in a variety of solvents, offers a route towards GO-based thin-film electronics and optoelectronics. The electrical and optical properties of GO are strongly dependent on its chemical and atomic structure and are tunable over a wide range via chemical engineering. In this Review, the fundamental structure and properties of GO-based thin films are discussed in relation to their potential applications in electronics and optoelectronics.

1. Introduction

Graphene is an atomically thin layer of sp^2 hybridized carbon atoms arranged in a honeycomb lattice. Observation of graphitic carbon monolayers by chemists[1] and surface scientists[2] date back to the 1960s. In 1986, Boehm et al.[3] referred to such single layers of graphite as graphene. However, exfoliation of graphite into individual graphene sheets remained a curiosity[4] until 2004, when isolated graphene using the simple Scotch tape method[5,6] was reported. The subsequent discoveries of its unusual properties[7,8] have led to an extraordinary amount of interest amongst researchers across virtually all scientific disciplines.[9,10]

Graphene is most often highlighted by physicists for its giant carrier mobility[11–13] and a range of unusual phenomena arising from the linear energy dispersion.[7,8,14–19] The rapid progress of the field, which resulted in the discovery of its extraordinary mechanical,[20] thermal,[21] chemical,[22,23] and optical properties[16,24] has also raised interest in disciplines other than condensed-matter physics, as discussed in recent reviews.[25–31] One branch of graphene research deals with chemically derived graphene (CDG), a material resulting from chemical exfoliation of graphite.[32–34] CDG is also a 2D form of carbon but with chemical moieties that render new functionalities while preserving some of the unique properties of the pristine material.

[*] Prof. M. Chhowalla, Dr. G. Eda
Department of Materials
Imperial College London
Exhibition Road, London SW7 2AZ (UK)
E-mail: m.chhowalla@imperial.ac.uk

DOI: 10.1002/adma.200903689

A major advantage of CDG is that it is straight forward to synthesize, process, and integrate into devices using existing planar thin-film-electronics techniques. Motivated by early work on graphite oxide and the effort to produce[4] and manipulate[35,36] graphene, Stankovich et al.[32–34] demonstrated a simple and scalable method for efficient production of CDG, which involves the chemical synthesis of graphite oxide, followed by its exfoliation into individual graphene oxide (GO) sheets, and their subsequent reduction. It should be clarified that in this Review, we define GO as graphene oxide and not graphite oxide. CDG has become a generic term for describing reduced GO (rGO) and its derivatives, while other forms derived from fluorinated[37] or brominated[38] graphite can also be included in this category. rGO is also referred to as functionalized graphene, chemically modified graphene, chemically converted graphene, or reduced graphene. The chemical exfoliation of graphite via oxidation leads to covalent functionalization, which dramatically alters the structure of graphene. Therefore, it is not appropriate to refer to GO or reduced GO simply as graphene since their properties are substantially different.

The covalent oxygen functional groups in GO give rise to remarkable mechanical strength[39,40] along with molecular-level chemical sensing capability.[41] The presence of functional groups also implies modification of the graphene electronic structure. Therefore, the chemical composition of GO, which can be chemically, thermally, or electrochemically engineered, allows tunability of its optoelectronic properties.[42,43] Although relativistic charge-carrier transport and other condensed-matter effects observed in nearly ideal graphene are absent in GO and rGO, accessibility, ease of processing, and the versatile properties make it attractive for fundamental research as well as for applications.

The production of GO/rGO outlined by Stankovich et al.[32] is attractive for several reasons. First, natural graphite, a ubiquitous and inexpensive resource is used as the raw material. Second, the yield of monolayer GO/rGO is high (>80%) due to efficient exfoliation so that a very small amount of bulk raw material translates into atomically thin films with giant surface areas. Third, the process is conducted in solution phase, allowing ease of thin-film deposition or fabrication of paperlike structures. Fourth, chemical process simplifies the integration of GO/rGO into composites with polymeric[34] or ceramic hosts.[44] In contrast, the production of graphene based on micromechanical cleavage or ''Scotch-tape'' peeling of highly oriented pyrolitic

graphite (HOPG) yields a low density of monolayer graphene, albeit of high crystal quality, among multilayers and graphitic platelets.[5] Growth of graphene via chemical vapor deposition (CVD)[45–49] (see Ref. [31] for a comprehensive review) and thermal decomposition of SiC[50–53] is being actively pursued, resulting in remarkable progress. However, the use of high temperature complicates the integration of graphene into practical device systems, especially on plastic substrates. Recently, solution-phase noncovalent exfoliation of graphite has been reported.[54–58] These methods are often compared with the chemical routes due to the similarity in the solution-based approach. However, it should be noted that, while the chemical approach aims to exploit new functionalities of GO/rGO, the nonchemical approaches have focused on the preservation of graphene properties.

Due to the processing advantages and unique properties such as mechanical stability, tunable electrical, and optical properties, GO/rGO is attractive for flexible and bendable thin-film electronics and opto-electronics,[42] where components of the devices are built on plastic or paperlike platforms. Analogous to carbon nanotube network electronics,[59] GO/rGO sheets can be assembled into layered network structures, which can be viewed as ''polycrystalline'' films where the single ''crystals'' are the individual sheets of GO/rGO. Numerous reports have appeared in the past 2 years, revealing the unique and sometimes unexpected optoelectronic properties of rGO-based thin films, providing prospects for their use as transparent conductors,[60–66] chemical/biological sensors,[41,67–71] thin-film transistors (TFTs),[42,72] electrodes,[73] ultracapacitors,[74] field emitters,[75] photovoltaics,[76–79] photo-detectors,[80] nanoelectromechanical resonators,[40] and nonvolatile memory devices.[81,82] In particular, recent studies address the importance of understanding the chemical and atomic structure of GO/rGO in achieving the desired optoelectronic properties.[43,83]

In this Review, the fundamental material properties of GO/rGO are summarized. Subsequently, key demonstrations of rGO-based thin-film devices are highlighted. The discussions emphasize the need for a better understanding of the structure–property relationship of the materials, which we believe to be the key for the development of high-performance devices. The chemistry of GO and rGO has been summarized in recent reviews[26,30] and, therefore, is not discussed in great detail here. Section 2 summarizes thin-film fabrication techniques along with morphological properties of the material. After reviewing the structural properties of GO and rGO in Section 3, device implementation, demonstration, and carrier-transport mechanisms are discussed in Section 4. Conclusions and prospects for future work are outlined in the final Section.

2. Fabrication of Thin Films

The scheme for the two classes of rGO-based thin films discussed in this Review is illustrated in Figure 1. Type one are pure rGO films, which consist of a percolating network of sheets lying flat on a substrate surface. Type two are composite films consisting of rGO as the filler and polymer or ceramic as the host material. The starting point for the fabrication of these films is the oxidation of graphite, which readily exfoliates in water, forming a colloidal suspension of GO. For electronic and optoelectronic applications discussed here, GO, which is electrically insulating, must be reduced to become electrically conductive.[34] Various methods of reduction have been reported, resulting in varying degrees of restored electrical conductivity. Similarly, thin-film-deposition techniques of GO/rGO influence the degree of coverage, number of layers, and surface morphology giving rise to a variety of properties. In the following Sections, synthesis, dispersion, reduction, and deposition of GO are discussed.

Manish Chhowalla is currently a Professor in the Department of Materials at Imperial College London. He was an Associate Professor and the Donald H. Jacobs Chair at Rutgers University, NJ, USA. He was a Royal Academy of Engineering Research Fellow at the University of Cambridge after completing his Ph.D. in Electrical Engineering at the same university in 1998. His research interests are in the synthesis and characterization of novel carbon materials and their incorporation into devices.

Goki Eda obtained his B.A. degree in Physics from the International Christian University in Tokyo in 2003. After receiving a M.S. degree in Materials Science and Engineering from Worcester Polytechnic Institute, MA (USA), in 2006, he obtained his Ph.D. in the same discipline from Rutgers University, NY (USA), in 2009. He is currently a Newton International Fellow at Imperial College London, studying the electronic and optoelectronic properties of graphene-based thin films and related materials for device applications.

2.1. Synthesis of Graphene Oxide

Synthesis of graphite oxide can be achieved by placing graphite in one or more concentrated acids in the presence of an oxidizing agent. Graphite oxide was first prepared almost 150 years ago by Brodie, who treated graphite repeatedly with potassium chlorate and nitric acid.[84] This method was modified by several investigators including Staudenmaier[85] and Hamdi[86] who used a mixture of sulfuric acid and nitric acid with potassium chlorate. Hummers and Offeman[87] later demonstrated a less hazardous and more efficient method for graphite oxidation, which involves a mixture of sodium nitrate, potassium permanganate, and concentrated sulfuric acid. These and their modified versions are presently the most commonly used methods for the oxidation of graphite.[88–91] Other methods such as electrochemical oxidation of graphite have also been reported.[92]

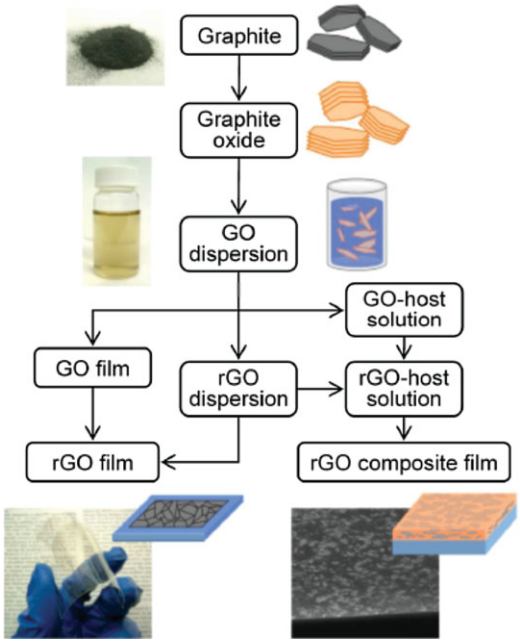

Figure 1. Process scheme for fabricating rGO-based thin films. The schematic illustrations show the structure of the material at each stage of the process. The gray and the orange sheets represent not oxidized and oxidized graphene sheets, repectively.

Graphite oxide in water hydrolyzes to form thin platelets, which are negatively charged. While Brodie[84] remarked that the platelets were "extremely thin," it was about 100 years later when Boehm et al.[1] concluded that the thinnest graphite oxide platelets consisted of single-carbon-thick layers. Today, the existence of monolayers of graphite oxide is widely acknowledged and recognized as graphene oxide (GO).[32,34] The term "platelets" is often used to describe thick multilayers of GO or rGO, while "sheets" usually indicate a monolayer to few layers.[93]

Individual sheets of GO can be viewed as graphene decorated with oxygen functional groups on both sides of the plane and around the edges as described by Lerf et al.[94,95] (Fig. 2a). Due to ionization of carboxyl groups, which are primarily present at the sheet edges (Fig. 2a), GO can be electrostatically stabilized to form a colloidal suspension[96] in water, alcohols, and certain organic solvents[97,98] without surfactants. Exfoliation of graphite oxide into individual sheets can be facilitated by ultrasonic agitation[33] or rapid heating[99,100] but excessive ultrasonication can result in decrease of lateral dimensions.[72,101]

Oxidation of graphite results in a brown-colored viscous slurry, which contains graphite oxide and exfoliated sheets along with nonoxidized graphitic particles and residue of the oxidizing agents. After repeated centrifugation, sedimentation, or dialysis, salts and ions from the oxidation process can be removed from GO suspensions (see for example, Ref. [42,89,96,102]). To achieve a suspension of monolayer GO, nonoxidized graphitic particles and thick graphite oxide platelets are precipitated out by further centrifugation. Suspensions of GO flakes that are monodispersed according to their lateral size can also be obtained by density-gradient centrifugation.[101]

The thickness of a monolayer GO sheet is approximately 1–1.4 nm, which is thicker than an ideal monolayer of graphene (thickness ~0.34 nm) due to the presence of functional groups and adsorbed molecules (Fig. 3a).[32,103] Since the functional groups make GO strongly hydrophilic, multilayered GO contains trapped water molecules between the layers.[94,103,104] Studies have shown that these molecules can be partially removed from the structure during thermal reduction [103,105] (Fig. 3b). Despite the difference in their optical properties, like pristine graphene,[106,107] GO sheets are also readily visible on Si substrates with 300-nm SiO_2 (Fig. 3c).[108] Furthermore, high-contrast visualization of GO on arbitrary substatrates can be achieved by fluorescence quenching microscopy.[109,110] The maximum lateral size of GO sheets is dependent on the size of initial graphite crystals, but the average size can be adjusted to some degree by the extent of oxidation procedure[111] or by ultrasonication.[72,101] Large and small GO sheets observed with optical and atomic force microscopy (AFM), shown in Figure 3c–e, respectively, demonstrate the wide range of lateral sizes. By using large graphite crystals as the starting material and employing a multistep oxidation process, GO sheets as large as 3 mm have been synthesized.[112] Due to the ease of identification on SiO_2/Si substrates and their large lateral size, GO sheets can be contacted with metal electrodes for electrical studies using standard lithographic techniques.[113] On the other hand, GO sheets having lateral sizes of few nanometers have also been observed after extensive ultrasonication.[101]

2.2. Reduction of Graphene Oxide

There are a number of routes for reduction of GO, as briefly summarized in recent reviews.[26,30] Chemical methods involve exposure of GO to reducing chemicals such as hydrazine (hydrazine monohydrate,[32,113,114] dimethylhydrazine,[34,42] and anhydrous hydrazine[115]), hydrides (sodium borohydride[116–119] and sodium hydride[120]), hydroquinone,[116,121] and *p*-phynylene diamine.[122] Reduction of GO also occurs in strongly alkaline environments[123] and in supercritical water.[124] Thermal reduction of GO is typically achieved above 200 °C in inert or reducing environments and becomes more efficient at higher temperatures.[60,61,125] It should be noted that in the presence of oxygen, GO decomposes quickly at high temperatures[32] and gradually at lower temperatures (<200 °C). Annealing GO in NH_3 atmosphere above 300 °C results in reduction as well as N doping via formation of C−N bonds.[126] Efficient chemical reduction of GO is achieved in solution, since both sides of the sheets can interact with the reducing agent while in thin films only the exposed regions are reduced.[102,127] Hydrazine is effective for the removal of in-plane functional groups such as epoxy and hydroxyls but leave the edge moieties such as carboxyl and carbonyl intact.[83,102,127] Gao et al.[83] demonstrated that these residual edge groups can be removed by additional exposure to concentrated H_2SO_4 after the initial reduction treatment. As an alternative to chemical methods, hydrogen plasma treatment has been also shown to result in efficient reduction.[113] Other routes include electrochemical reduction,[128–130] photocatalytic reduction,[131] and flash conversion,[70] but no comparative studies on their reduction efficiencies have been conducted.

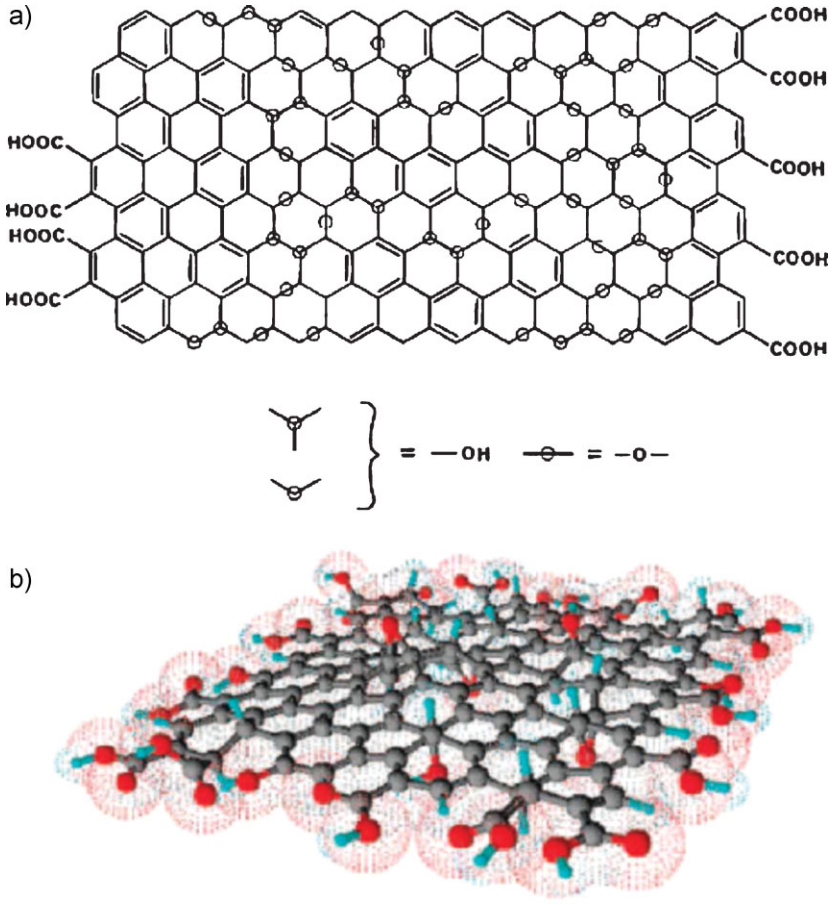

Figure 2. a) Chemical structure model of GO. Position of oxygen functional groups are indicated by circles. The functional groups are attached on both sides of the graphene sheet. Reproduced with permission from [94]. Copyright 1998, American Chemical Society. b) 3D view of a GO sheet. In reality, the sheets are corrugated due to puckering caused by the functional groups. Reproduced with permission from [96]. Copyright 2009, American Chemical Society.

Multistep reduction based on a combination of different processes is also an effective route for removing specific functional groups.[83] The present reduction methods utilizing hydrazine and high-temperature annealing are not ideal for environmental and technological reasons, respectively.

Efficiency of the reduction process depends largely on the methods and various parameters used.[43] However, none of the reported reduction methods yield complete removal of oxygen, resulting in only partial restoration of sp^2 conjugated graphene network. In addition, thermal reduction processes lead to the creation of vacancies in the basal plane due to the evolution of carbon in the form of CO or CO_2.[99,132] Although it has been argued that hydrazine reduction proceeds without evolution of carbon,[32] experimental evidence for this is been available. The structure of chemically and/or thermally reduced GO has not been widely investigated theoretically[133,134] and, therefore, information regarding residual oxygen groups in rGO is limited. However, it is known that residual C—O sites and vacancies introduce substantial disorder in rGO, which hinders charge transport through the atomically thin plane. The atomic and electronic structures of GO and rGO are discussed in Section 3 and their ramification on the optoelectronic properties are described in Section 4.

2.3. Thin-Film Deposition

GO sheets can be deposited on virtually any substrate in the form of thin films using techniques such as drop-casting,[99,113] dip-coating,[60] spraying,[135] spin-coating,[40,41,61,73,136] electrophoresis,[122,127] Langmuir–Blodgett (L–B)[96,137]/Langmuir–Schaefer[138] and transfer via vacuum filtration.[42,43,62] Control over film uniformity, surface morphology, thickness, and surface coverage depend on the deposition methods and parameters used. Drop-casting, dip-coating, and spraying often result in nonuniform deposition due to aggregation of GO, allowing poor control over the film thickness. Once deposited, the van der Waals forces are sufficient to keep the GO sheets strongly adhered to the substrate.[42] Individual sheets are held together with strong hydrogen bonding, which also helps the films adhere to hydrophilic surfaces.[40] To encourage adhesion on glass substrates, their surfaces can be treated with acid[96,136] or (aminopropyl)triethoxysilane (APTES) prior to deposition.[61]

For spin-coating, GO suspensions with relatively high concentrations (0.5–3 mg mL^{-1}) are required to yield uniform continuous films.[40,41,61,73] Rapid evaporation of solvent during spin-coating is critical to allow greater interaction between the GO sheets and the substrate surface, thereby increasing the adhesion (Fig. 4a). Spin-coating typically results in the deposition of films with minimal wrinkling. Film thicknesses can be controlled by adjusting the GO concentration or number of spin-coating cycles (Fig. 4c). Through careful control of the solvent evaporation rate, deposition of uniform GO films on ~30 cm wafers has been demonstrated.[136]

Vacuum filtration has been frequently used for the fabrication of GO films[42,43,62] and free-standing papers.[39,139] The vacuum filtration method has also been utilized to make uniform thin films of single-walled carbon nanotubes (SWNTs) for transparent and flexible devices.[140–142] To obtain thin films of GO, suspensions with relatively low concentrations (~0.5 mg L^{-1}) are filtered through mixed cellulose ester membranes (MCE) with nanometer-sized pores. As the suspension is passed through the ester filter, the liquid is able to pass through the pores with the aid of a vacuum pump while the GO sheets become lodged, leading to the deposition of a film on the membrane (Fig. 4b). The process allows reasonably good nanometer-scale control over the film thickness and percolation of sheets in sub-monolayer films. The GO films can then be transferred onto various substrates by gently pressing the film against substrate surface and dissolving the ester membrane[42] (Fig. 4d and e).

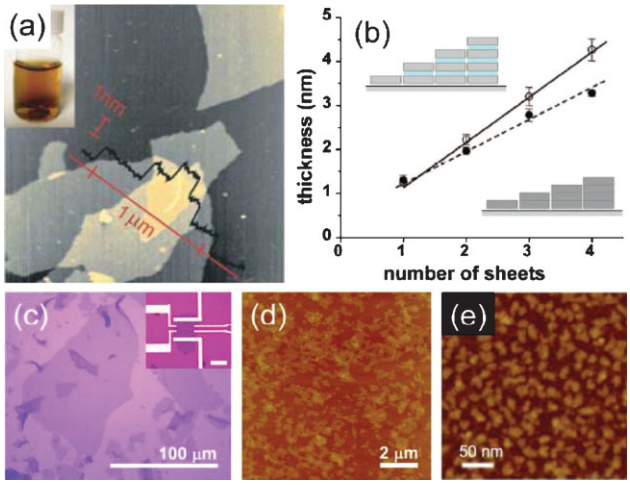

Figure 3. a) AFM image of overlapping GO sheets. The height profile shows that the thickness of individual GO sheets is approximately 1 nm. The inset shows a photograph of a GO suspension in water. Reproduced with permission from [34]. Copyright 2006, Nature Publishing Group. b) Thickness of GO sheets measured by AFM as a function of the number of layers before (open circles) and after (solid circles) thermal reduction. The inset shows schematic illustration of mono- and multilayer GO (above) and rGO (below) sheets showing an intercalating water layer in GO and interfacial layer between the GO/rGO sheets and the substrate. Reproduced with permission from [103]. Copyright 2008, American Chemical Society. c) Optical microscopy image of large GO sheets deposited on a SiO_2/Si substrate. d) AFM image of submicrometer-sized GO sheets. Reproduced with permission from [72]. Copyright 2009, American Chemical Society. e) Nanometer-sized GO sheets obtained by extensive sonication. Reproduced with permission from [101]. Copyright 2008, Springer.

L–B assembly has been used for controlled deposition of highly uniform GO films[96,137] (Fig. 4f). This technique exploits the electrostatic repulsive forces between the ionized edge functional groups of individual GO sheets.[102] Briefly, a suspension of GO in a mixture of water and methanol is carefully spread over the water surface to obtain floating GO sheets trapped at the water/air interface. The density of GO sheets can be controlled by varying the available water/air interface area. Since the GO sheets are electrostatically stabilized, they remain dispersed as monolayers with decreasing area until the edge-to-edge repulsive forces are overcome by the attractive forces between sheet faces, leading to stacking of layers.[96] The floating GO film is deposited onto a substrate as it is slowly raised out of the solution.

GO thin films deposited on SiO_2/Si substrates can also be transferred onto other substrates via delamination in water. Robinson et al.[40] demonstrated that treatment of GO films with sodium hydroxide solution and subsequent dipping in water leads to uniform delamination of free standing films floating on the water surface. The film can then be recaptured onto a desired substrate (Fig. 5g). An additional polymer support layer can be deposited to ensure that the film does not disintegrate into individual sheets during transfer.[136]

Spin-coated films are generally highly continuous and cover the entire substrate (Fig. 5a), while L–B assembly is suited for producing highly uniform, close-packed monolayered GO films in the subpercolation regime (Fig. 5c). Vacuum filtration allows deposition of films with wide-ranging thicknesses but often with pronounced wrinkling, especially in the case of thick films ($N \gg 5$)[143] (Fig. 5d). Patterning of GO films can be achieved using standard lithographic processes. Deposition of a patterned sacrificial masking layer followed by oxygen plasma etching can preferentially remove GO from unprotected regions[41,73] (Fig. 5e and f). Selected-area vaporization of GO via laser ablation allows mask-free direct patterning of films.[144]

3. Structural Properties

The determination of GO structure has been challenging because of its non-stoichiometric chemical composition, which depends on the synthesis method and the degree of reduction. Some of the key questions pertaining to the structure of GO are: i) Which functional groups are present? ii) What are the amount of and iii) relative fraction of the functional groups? iv) How are they distributed spatially over the graphene plane? v) And finally, how do they evolve during reduction? Various structural models of GO have appeared in the literature over the past several decades, as summarized in Reference [145]. The recent breakthrough in the solid-state NMR characterization of ^{13}C-labeled graphite oxide[146] and other similar works[83,147,148] have indicated that the most probable chemical configuration is described by the Lerf-Klinowski [94] and the Dékány models[145] with minor modifications, providing satisfying answers to questions i–iii. raised above. However, the information obtained via analytical studies is not sufficient for fully understanding the optical and electrical properties of GO/rGO, which are critically dependent on the spatial distribution of the functional groups. For example, the electron mean free path is limited by the distance between two defective sites represented either by C—O or a vacancy.[149] Understanding the evolution of the GO structure during reduction is therefore critical. From this perspective, the following Sections review studies discussing the atomic- and nanometer-scale characterization of GO.

3.1. Chemical Structure

The oxygen functional groups in GO have been identified by various techniques.[150] It is generally agreed that oxygen is present in GO mostly in the form of hydroxyl and epoxy groups on the basal plane, whereas smaller amounts of carboxyl, carbonyl, phenol, lactone, and quinone are present primarily at the sheet edges. Depending on the preparation method, GO with chemical compositions ranging from $C_8O_2H_3$ to $C_8O_4H_5$, corresponding to a C:O ratio of 4:1 to 2:1 is typically produced.[150–153] After reduction, the C:O ratio can be improved to approximately 12:1 in most cases[43,99] but values as large as 246:1 have been recently reported.[83] Simulations based on density functional theory (DFT) have indicated that it becomes increasingly difficult to reduce GO with C:O ratios above 16:1.[154]

Another important parameter that can be used to characterize the degree of oxidation or reduction in GO is the sp^2 carbon fraction. Since it is the π-electrons from the sp^2 carbon that largely determine the optical and electrical properties of carbon-based materials,[155] the fraction of sp^2 bonding can provide insight into the structure–property relationships. Carbon atoms bonded with

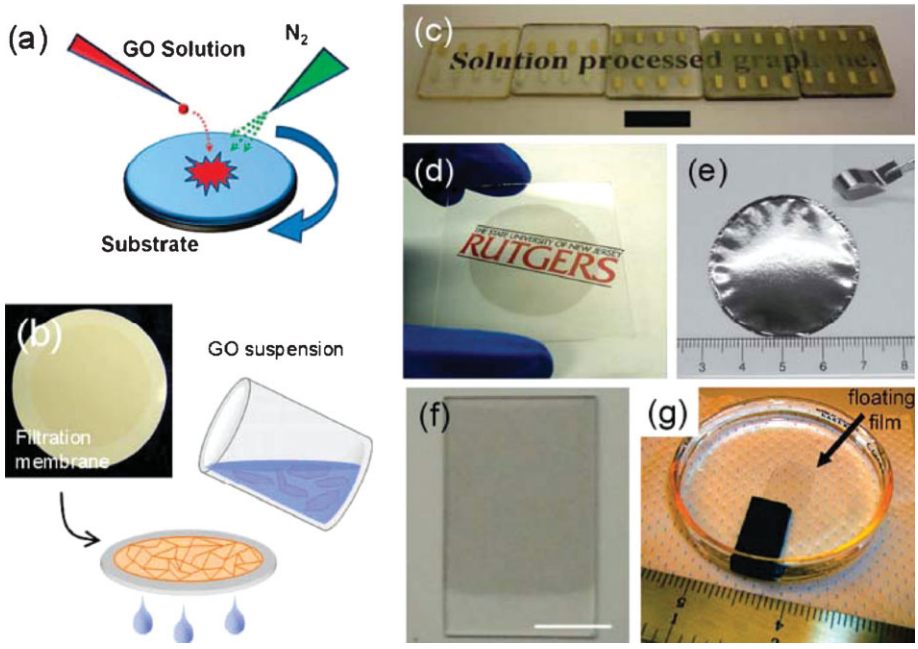

Figure 4. a) Schematic illustration of spin-coating deposition of GO thin films. The N_2 jet is used to facilitate solvent evaporation during deposition. Reproduced with permission from [40]. Copyright 2008, American Chemical Society. b) Schematic illustration of the filtration of a GO suspension. The photograph shows the GO film captured on the filtration membrane. Reproduced from with permission [42]. Copyright 2008, Nature Publishing Group. c) Photograph of the as-deposited GO film (leftmost) and a series of thermally reduced GO films with increasing thickness on quartz substrates. The scale bar is 1 cm. Reproduced with permission from [61]. Copyright 2008, American Chemical Society. d) Photograph of a large-area rGO film (10 cm in diameter) on glass obtained via a vacuum-filtration method. Reproduced with permission from [42]. Copyright 2008, Nature Publishing Group. e) Photograph of a vacuum-filtered 10-μm-thick rGO film exhibiting a shiny metallic luster. Reproduced with permission from [102]. Copyright 2008, Nature Publishing Group. f) Photograph of a L–B CDG film. The scale bar is 10 mm. Reproduced with permission from [137]. Copyright 2008, Nature Publishing Group. g) Photograph of a rGO film released onto water surface. The film has the same dimension as the parent substrate seen on the bottom of the petri dish. Reproduced with permission from [40]. Copyright 2008, American Chemical Society.

hydroxyl and epoxy groups are sp^3 hybridized and thus are dominant in as-synthesized GO. It should be noted that the C:O ratio does not directly translate into an sp^2 fraction, because one hydroxyl group is attached to one sp^3 carbon, whereas one epoxy group is attached to two sp^3 carbon atoms. Further, the relative fraction of these groups may vary with different methods of oxidation.[26] Mattevi et al.[43] have recently shown with XPS analysis that the sp^2-bonded carbon fraction increases from ~40% in pristine GO to ~80% in thermally reduced GO.

3.2. Atomic Structure

An ideal sheet of graphene consists of only trigonally bonded sp^2 carbon atoms and is perfectly flat,[156] apart from the microscopic ripples.[157] On the other hand, a GO sheet consists partly of tetrahedrally bonded sp^3 carbon atoms, which are displaced slightly above or below the graphene plane.[99] Due to the structural deformation and covalently bonded functional groups, GO sheets are atomically rough.[98] Despite the presence of atomic-scale protrusions, the GO sheets can efficiently stack on one another[158] leading to graphite-like layered structure, or graphite oxide (Fig. 6a). The interlayer spacing depends on the relative humidity due to the hygroscopic nature of GO and ranges from ~0.6 to ~1.2 nm for dry and hydrated samples.[104] During thermal reduction, the trapped water molecules diffuse out of the structure and the functional groups evolve as gases, thereby leading to slight shrinking of the interlayer spacing.[103,105] Removal of carbon from the GO backbone generates defects such as double vacancies, often referred to as 5–8–5 defects, and Stone–Wales or 5–7–7–5 defects.[99,159]

Carbon materials consisting of both sp^2-and sp^3-hybridized atoms are typically amorphous, possessing poor or no translational symmetry.[155] Surprisingly, reports show that the graphene-like honeycomb lattice in GO is preserved, albeit with disorder, consistent with the early studies on graphite oxide indicating its crytalline nature.[160,161] That is, the carbon atoms attached to functional groups are slightly displaced but the overall size of the unit cell in GO remains similar to that of graphene. GO is therefore structurally similar to partially hydrogenated graphene (or ''graphane''), which possesses the original honeycomb lattice structure despite the presence of both sp^2 and sp^3 carbon.[23] The transmission electron microscopy (TEM) image of a GO monolayer (Fig. 6b) indicates its high transpancy to the electron beam in comparison to the thin amorphous carbon support. The sharp selected-area electron diffraction (SAED) spot patterns of the GO monlayer reveals that the crytalline order of the original graphene lattice is present over at least a few nanometers[162] (Fig. 6c). Wilson et al.[162] further remarked that the long-range orientational order is also present over the the entire sheet (several micrometers in size). The SAED analysis from bilayers reveal two misoriented hexagonal patterns, indicating incommensurate stacking of the GO sheets (Fig. 6d). This is not surprising as the functional groups protruding from the GO planes are expected to decouple the interactions between the carbon backbones of neighboring layers.[158,162] Evidence of AB stacking has been reported for multilayered GO,[153] however, it is possible that such samples are incompletely oxidized graphitic platelets with little or no interlayer oxygen. This must be distinguished from overlapped or stacked monolayers. High-resolution TEM (HR-TEM) has been used to image the honeycomb lattice along with disorder in GO[162] (Fig. 6e).

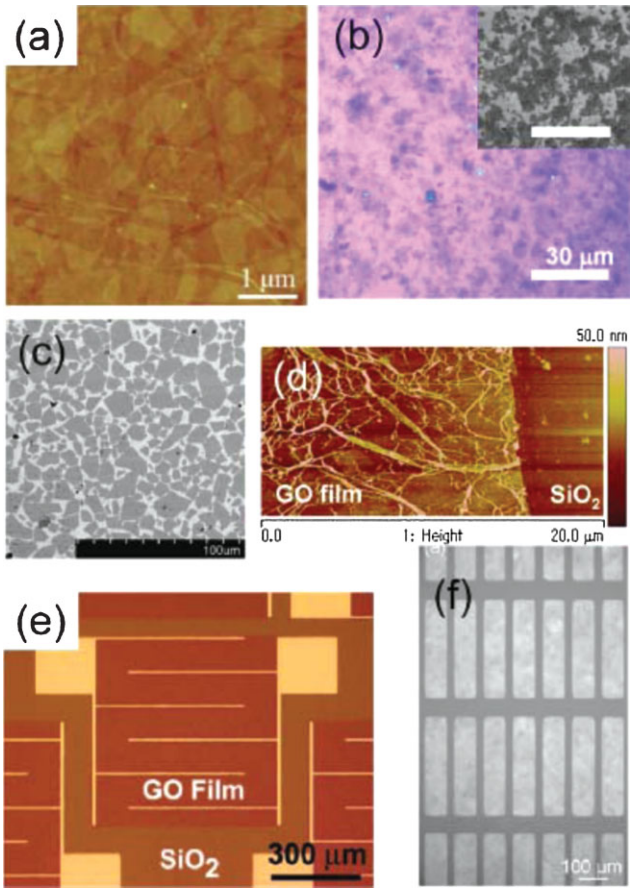

Figure 5. a) AFM image of 20 nm-thick spin-coated GO film on silicon substrate. Reproduced from [73]. Copyright 2009, Wiley-VCH. b) Optical microscopy image of a percolating network of rGO sheets on a SiO_2/Si substrate prepared by vacuum filtration. The corresponding SEM image shown in the inset shows the contrast between the conductive rGO and the insulating substrate. Reproduced with permission from [42]. Copyright 2008, Nature Publishing Group. c) SEM image of a subpercolating GO network deposited via L–B method. Reproduced with permission from [96]. Copyright 2009, American Chemical Society. d) AFM image of GO film exhibiting extensive surface wrinkles prepared by a vacuum filtration method.[143] e) Optical microscopy image showing a patterned rGO film with interdigitated Ti/Au electrodes used for molecular-sensing studies. Reproduced with permission from [41]. Copyright 2008, American Chemical Society. f) Optical microscopy image of patterned rGO electrodes for organic thin-film transistors. Reproduced from [73].

Oxygen functional groups of GO are uniformly but randomly attached on the graphene plane. Mkhoyan et al.[158] recently examined the oxygen distribution on a GO monolayer using high-resolution annular dark field (ADF) imaging in a scanning transmission electron microscopy (STEM) instrument, as shown in Figure 6f. The results indicate that the degree of oxidation fluctuates at the nanometer-scale, suggesting the presence of sp^2 and sp^3 carbon clusters of a few nanometers. Several groups[113,159,163] have studied the surface of GO with scanning tunneling microscopy (STM) and observed highly defective regions, probably due to the presence of oxygen and other areas that were nearly intact (Fig. 7a and b). Fourier transformation of the STM images reveals long-range crytalline order consistent with TEM observations.[159] Pandey et al.[164] examined the oxidized regions and, surprisingly, observed a periodic arrangement of oxygen atoms, which spanned over a few nanometers (Fig. 7b). The oxygen atoms were arranged in a rectangular lattice, suggesting a series of epoxy groups present in strips (Fig. 7c). Such arrangement of epoxy groups is energetically favorable according to DFT calculations.[165] This observation, however, is inconsistent with the SAED results, which indicate that the oxygen atoms do not form periodic structures.[162]

Nanometer-scale surface corrugations of GO and rGO sheets deposited on HOPG have been recently examined using AFM.[101,163] Paredes et al.[163] showed that GO and rGO sheets exhibit globular morphology with feature sizes ranging from 5 to 10 nm (Fig. 7e and 7f). The surface roughness of GO was found to be approximately 0.1 nm. It is tempting to attribute this roughness to the C–O groups protruding from the carbon backbone, as the C–O bond length[166] coincides with this length scale. Although some similarities can be found between the topographic image shown in Figure 7e and the oxygen distribution map from the ADF image (Fig. 6f), the length scale of the fluctuations differs appreciably, suggesting that the observed undulations of GO and rGO are associated with carbon backbone distortions rather than the functional groups.

3.3. Raman Spectroscopy

Raman spectroscopy is a non-destructive technique that is widely used to obtain structural information about carbon-based materials.[167] The main features in the Raman spectra of graphitic carbon-based materials are the G and D peaks and their overtones. The first-order G and D peaks, both arising from vibrations of sp^2 carbon, appear at around 1580 and 1350 cm^{-1}, respectively. The G peak corresponds to optical E_{2g} phonons at the Brillouin zone center and is due to bond stretching of sp^2 carbon pairs in both rings and chains. The D peak is due to the breathing mode of aromatic rings and requires a defect for its activation.[168] The D-peak intensity is therefore often used as a measure for the degree of disorder.[167] The overtone of the D peak, called 2D peak, appears around 2680 cm^{-1}, and its shift and shape has been correlated with the number of graphene layers (N).[169–171] The 2D peak is attributed to double resonance transitions resulting in production of two phonons with opposite momentum. Furthermore, unlike the D peak, which is only Raman active in the presence of defects, the 2D peak is active even in the absence of any defects.

Typical Raman spectra of monolayers of GO and rGO obtained at an excitation wavelength of 532 nm are shown in Figure 8. The general features of the spectra for GO are similar to those seen in partially hydrogenated graphene[23] but deviate from those of mechanically exfoliated graphene, where the D peak is absent and the peaks are more clearly defined.[172] The prominent D peak (~1350 cm^{-1}) with intensity comparable to the G peak (~1600 cm^{-1}) along with their large band width are indicative of significant structural disorder in GO. Weak and broad 2D peaks are another indication of disorder.[173] It should be noted that for mechanically exfoliated graphene, the 2D peak is sharp with FWHM of ~30 cm^{-1} (as opposed to ~200 cm^{-1} for GO) and

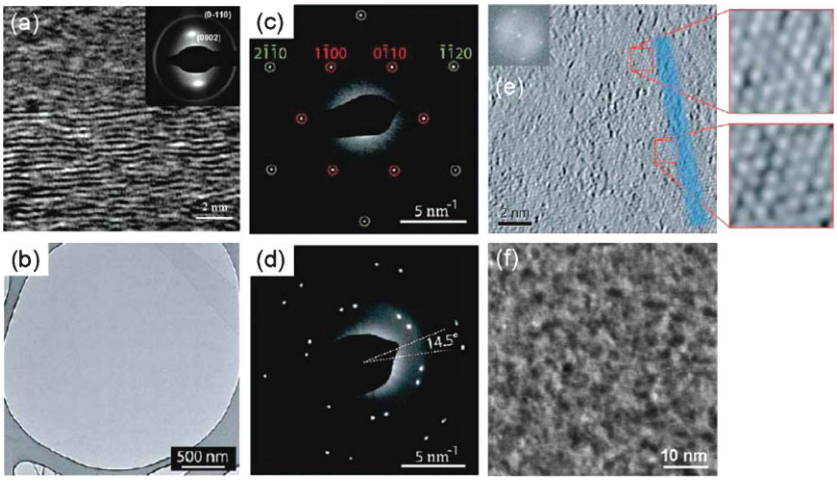

Figure 6. a) TEM image and corresponding SAED pattern (inset) of a thick rGO film. Reproduced with permission from [60]. Copyright 2007, American Chemical Society. b) TEM image of a monolayer GO flake. SAED pattern of c) a monolayer and d) a bilayer region of a GO flake. e) High-resolution TEM image of a monolayer GO. The inset shows the Fourier transform of the image. Reproduced with permission from [162]. Copyright 2009, American Chemical Society. f) ADF image of a GO monolayer showing contrast between oxygen-free and oxidized regions. Reproduced with permission from [158]. Copyright 2009, American Chemical Society.

exhibits higher intensity than the G peak.[172] A defect-activated peak called D + D' is also readily visible near 2950 cm^{-1} (Ref. [23]). The overall Raman peak intensities are diminished after reduction treatment, suggesting loss of carbon during reduction (not illustrated in Fig. 8).[143,174]

The G peak of GO and rGO is shifted to higher frequencies with respect to that of graphene and graphite. This G-peak stiffening is often associated with doping effects.[175] Indeed, a doping-induced G-peak shift in as-synthesized GO has been identified in ionic screening[176] and charge-transfer[177] studies. However, the fact that G-peak stiffening is commonly observed in GO and defective graphene[149] but not in mechanically exfoliated graphene under similar conditions suggests that other effects related to disorder may play a more significant role. A possible interpretation of the G-peak stiffening is based on the presence of isolated short double-bond segments.[167] Kudin et al.[159] simulated the Raman spectra of GO with various oxygen distributions and found that the blue shift of the G peak is possible if alternating single–double bond segments are present within

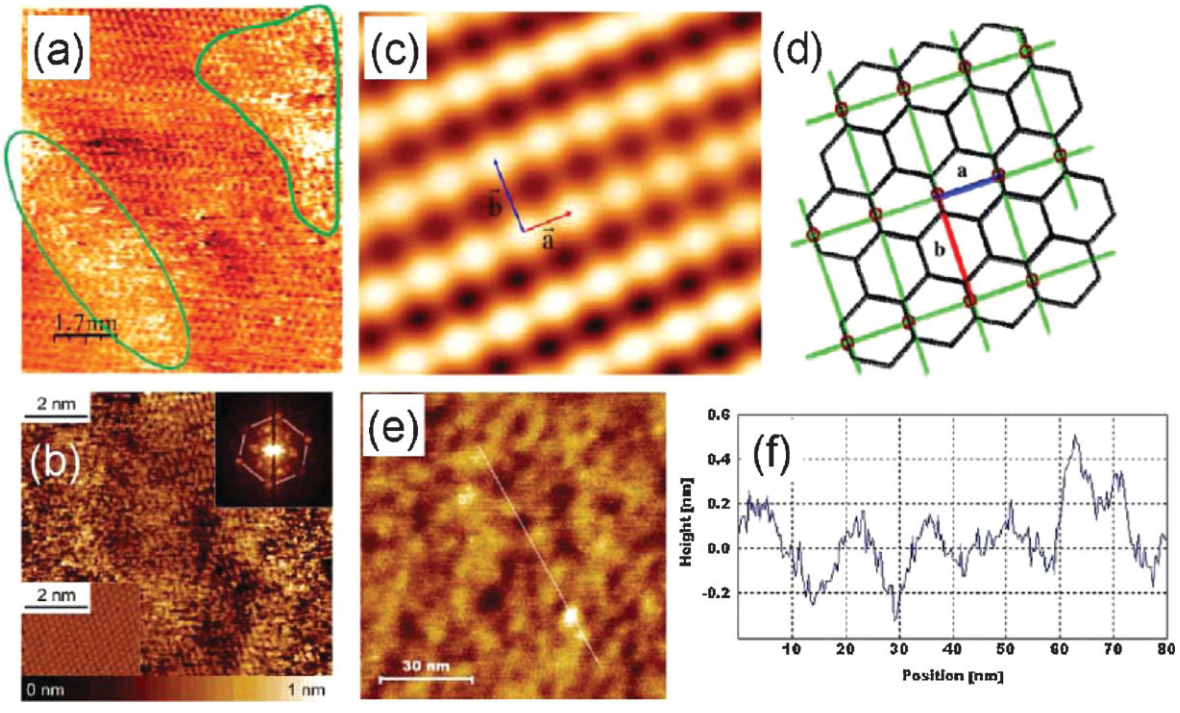

Figure 7. a) STM image of a GO monolayer on a HOPG substrate. Regions enclosed by green contours are populated with oxygen functional groups. Reproduced with permission from [113]. Copyright 2007, American Chemical Society. b) STM image of a rGO monolayer on a HOPG substrate and its Fourier transform (upper-right inset). The lower-left inset shows a STM image of a HOPG surface obtained under identical conditions. Reproduced with permission from [159]. Copyright 2008 American Chemical Society. c) High-resolution STM image of the oxidized region of GO revealing a rectangular lattice. The size of the lattice vectors *a* and *b* correspond to 0.273 and 0.406 nm, respectively. d) Schematic image of the rectangular lattice formed by a series of epoxy groups. Reproduced with permission from [164]. Copyright 2008, Elsevier. Tapping mode AFM e) height image and corresponding height profile (f) of GO on HOPG. Reproduced with permission from [163]. Copyright 2009, American Chemical Society.

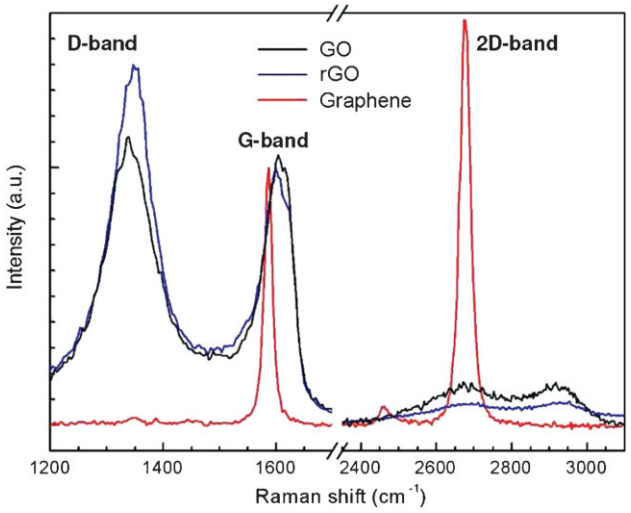

Figure 8. Raman spectra of a monolayer of GO, rGO, and mechanically exfoliated graphene on SiO_2/Si substrates normalized to the G-peak intensity. Reproduced with permission from [186]. Copyright 2008, American Chemical Society.

nanoribbon-shaped clusters of sp^2 carbon. However, such specific structures in GO do not agree with TEM observations. The origin of the G peak blue shift therefore requires additional clarification.

The 2D peak intensity in GO and rGO is typically weak and careful data acquisition is necessary to study its characteristics.[42] Nevertheless, the position of the 2D peak for GO and rGO is consistent with that of the monolayer of mechanically exfoliated graphene.[169] In commensurately stacked multilayers of graphene, the 2D peak splits into two major and two minor components due to coupling between the layers.[169,171] Their positions slightly blue-shift with increasing N up to $N \sim 5$ when the features are difficult to distinguish from those of graphite. The 2D-peak splitting in rGO spectra has been reported[42] but is often absent, probably due to weak interlayer coupling.[178] In multilayered GO, the 2D peak has been found to blue-shift with reduction, suggesting stronger interlayer coupling accompanied by removal of trapped interlayer species and functional groups.[179]

During thermal reduction, GO undergoes structural changes due to evolution and rearrangement of oxygen and carbon atoms. Such structural changes have been investigated by in situ and ex situ Raman spectroscopy for GO subjected to thermal annealing at various temperatures.[43,179] It is well documented[168,180–182] that the area ratio of the D and G peaks is a measure of the size of sp^2 ring clusters in a network of sp^2 and sp^3 carbon. Using the empirical Tuinstra–Koenig relation,[168] the average graphitic domain size in as-synthesized GO has been calculated and values ranging from 2.5 to 6 nm have been reported.[43,113] These values are in reasonable agreement with the size of the spatial fluctuations in oxygen (Fig. 6d), as discussed above. Variable effects of reduction on the sp^2 domain size in GO have been reported in the literature. The D/G ratio has been reported to increase,[32,115,163] decrease,[120,127,183] remain nearly constant,[43,113] or decrease following an increase.[83,184] In all cases, appreciable D-peak signal has been observed, indicating that significant disorder remains in the reduced sample. Mattevi et al.[43] reported that the D/G ratio remains nearly constant before and after thermal reduction and is independent of the annealing temperature. This observation suggests that even when the sp^2 sites are restored by de-oxidation, reduction does not lead to an expansion of the original sp^2 clusters. This is only possible if the sp^2 sites generated by reduction are isolated from the originally present sp^2 clusters by defects such as vacancies or residual sp^3 carbon. Understanding the discrepencies in the reported results requires further consideration into the reduction mechanism as well as optical cross-section of sp^2 clusters of various configurations.

It should also be noted that the applicability of the Tuinstra–Koenig relation should be carefully checked as it is not valid above a critical defect density. In highly disordered amorphous materials, where the sp^2 cluster size is smaller than ~2 nm, the D/G ratio increases with the number of aromatic rings, opposite to what is expected from the Tuinstra–Koenig relation. It has been shown recently[112] that the 2D/G ratio can be also used as the measure of order. This parameter has been found to correlate better with the carrier mobility.[112]

4. Electronic and Optoelectronic Properties

The properties of GO and rGO thin films can be tuned by varying the coverage of sheets, film thickness, chemical composition, average flake size, and film morphology. Unlike SWNTs, which are inhomogenous due to diameter- and chirality-dependent electronic properties, individual sheets of GO and rGO exhibit nearly identical properties.[113,185,186] Instead, the properties of GO and rGO depend heavily on their chemical and atomic structures. By appropriately tuning the deposition and reduction parameters, the films can be made insulating, semiconducting, or semimetallic, while maintaining optical transparency. Further, incorporation of rGO sheets into composites allows exploitation of rGO-host interactions, offering additional degrees of freedom in device functions.

It is well established that an ideal sheet of graphene is a zero-gap semiconductor.[9] The valence and the conduction bands of graphene meet at the Fermi energy, where the density of states (DOS) of the two bands vanishes linearly.[187] In multilayered graphene, overlap of the two bands gives rise to finite DOS at the Fermi level, rendering it semimetallic.[188] In contrast to the large body of work devoted to understanding the electronic structure of graphene and graphite,[189] little attention has been devoted to equivalent information on GO and rGO and their multilayers due to complications arising from structural disorder. The fundamental properties of GO and rGO such as the energy bandgap have not yet been well understood until recently. In the following Sections, experimental results providing insight into the electronic structure and transport properties of GO and rGO are highlighted, while discussing their manifestation in device properties.

4.1. Optical Properties

A suspension of GO in water is dark brown to light yellow, depending on the concentration, whereas that of rGO appears black, indicating appreciable differences in the electronic

structure. Similar changes in the physical appearance are also observed in thin films. When rGO films are sufficiently thin (<30 nm), they are semitransparent, while much thicker films appear opaque with graphite-like luster (Fig. 4e). The optical transmittance of GO and rGO films can be continuously tuned by varying the film thickness or the extent of reduction.[42] From UV–vis–IR spectroscopy studies, it can be inferred that the optical absorption of GO is dominated by π–π* transitions, which typically give rise to an absorption peak between 225 and 275 nm (4.5–5.5 eV).[190] The contribution of conduction electrons is minimal in the visible/near-UV photon energy range. The absorption spectrum of GO shown in Figure 9a is characterized by the π–π* plasmon peak near 230 nm and a shoulder around 300 nm often attributed to *n*–π* transitions of C=O.[163,191] No clear absorption edge is observed, suggesting absence of a well-defined bandgap. Upon reduction, absorption increases while the plasmon peak red-shifts to ~270 nm, reflecting increased π-electron concentration and structural ordering,[190] consistent with the restoration of sp^2 carbon and possible rearrangement of atoms. Similar features and trends are observed for GO films deposited on substrates.[192]

GO suspensions in water as well as in films are photoluminescent under illumination by visible and UV light sources.[101,192–195] Two distinct types of photoluminescence (PL) have been reported to date. The first type is a broad PL covering visible to near-IR range often exhibiting maximum intensity between 500 and 800 nm (1.55–2.48 eV; Fig. 9b).[101,193,194] The second type is blue emission, centered around 390 to 440 nm (2.82–3.18 eV) and is observed upon excitation with UV light.[192,195] The origin of the two different kinds of PL is still being debated but it has been suggested that the type of PL could be related to the state of dispersion.[192] No absorption features are observed in the PL-energy range (Fig. 9a), and thus the PL cannot be directly correlated with the bandgap of the material. Nevertheless, the energies of visible-to-near-IR PL coincide with the bandgap values of graphite oxide estimated from diffuse reflectance measurements, which range from 1.7 to 2.4 eV depending on the degree of oxidation.[196] DFT calculations predict the bandgap of GO to be in this range,[154,197,198] but scanning tunneling spectroscopy (STS) studies have yielded lower values of around 0.25 eV.[164] Interestingly, the PL spectrum is found to be independent of the GO sheet size and no obvious peak shift is observed even when the GO sheets are cut down to few nanometers in size.[101] This observation clearly indicates that the PL in GO is ascribed to the atomic-scale structure of the material and that the size of the sheet does not define the electron confinement, in contrast to the case of SWNTs where PL wavelength is strongly dependent on the tube diameter.[199] Thus, GO is expected to possess a range of local energy gaps across the sheet, giving rise to the broad PL. The behavior of the PL upon gradual reduction of GO is also distinctly different in the two systems, suggesting that the origin of the two types of PL is also different.[192] The common trend is that the PL intensity is quenched upon extensive reduction.

Considering the fact that the structure of GO is characterized by the nanometer-scale sp^2 carbon clusters, as discussed in Section 3, electron confinement in such clusters is possible because sp^3 carbon sites act as large repulsive barriers for carriers.[193] In such cases, the energy gap of the cluster is inversely related to its size.[155] Raman analysis and the STEM-ADF observations indicate the sp^2 cluster size to be 2.5–6 nm.[43,113,158] Assuming that their shape is circular, these clusters contain approximately 100 to 500 aromatic carbon rings. Using the semiempirical relationship $E_g = 2|\beta|M^{-0.5}$, which relates the number of aromatic rings (M) to the energy gap (E_g) with the nearest-neighbor interaction energy ($\beta \sim -2.9$ eV),[155] the energy gaps of sp^2 clusters of sizes 2.5 and 6 nm range from 0.58 to 0.24 eV, respectively. These values are significantly lower than the observed PL energies, suggesting that carrier confinement in such sp^2 clusters is not the origin of the PL. The energy gap giving rise to PL may thus arise from even smaller fragments of sp^2 carbon, which are not captured in Raman analysis.

Studies have also suggested that PL in GO is due to electronic states associated with zigzag edges[195] and chemical species[200] rather than "bulk", however, experimental evidence to verify such arguments is presently lacking. Other energy gap opening mechanisms based on topological disorder and vacancies also deserve attention in future work as possible mechanisms for PL.[193]

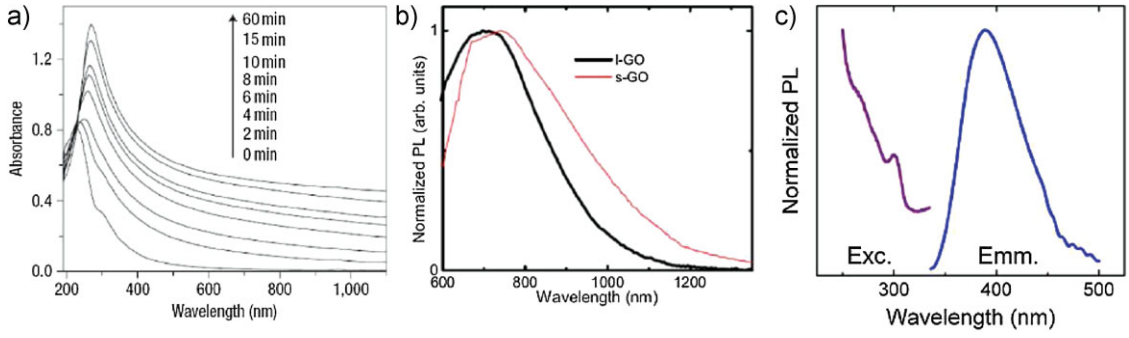

Figure 9. a) UV–vis absorption spectra of GO in water as a function of elapsed time during chemical reduction by hydrazine. Reproduced with permission from [102]. Copyright 2008, Nature Publishing Group. b) PL spectra of a GO suspension in water (l-GO) and a GO film on a substrate (s-GO), excited at 500 nm. Reproduced with permission from [193]. Copyright 2009, American Institute of Physics. c) PL emission spectrum for excitation at 325 nm and excitation spectrum for emission at 388 nm for a GO thin film reduced by hydrazine for 3 min (data from ref. [192]).

4.2. Electrical Conductivity

As-synthesized GO films are typically insulating, exhibiting sheet resistance (R_s) values of about $10^{12}\,\Omega$ sq^{-1} or higher.[61] An exception is when GO is synthesized by carefully minimizing the oxidation level such that as-synthesized GO film is semiconducting.[201] The insulating nature of GO is attributed to the absence of percolating pathways among sp^2 carbon clusters to allow classical carrier transport to occur. Reduction of GO results in decrease in R_s by several orders of magnitude.[186] Measurements on an individual sheet of rGO show that even in well-reduced samples (annealed at 1000 °C in H_2), the sheet resistance is 0.34 MΩ sq^{-1},[183] which is two orders of magnitude higher than that of ideal dopant-free graphene.[7] This is attributed to disorder arising from residual oxygen functional groups and presence of defects generated by evolved carbon. López et al.[185] recently demonstrated that vacancies can be "repaired" partialy by exposing rGO to a carbon source such as ethylene at elevated temperatures (800 °C), similar to conditions used for CVD growth of SWNTs. With this post-reduction deposition of carbon, the sheet resistance of individual rGO sheet can be decreased to 28.6 kΩ sq^{-1} with a corresponding conductivity of 350 S cm^{-1}.[138,185] Su et al.[65] reported a similar defect healing effect for rGO sheets functionalized with aromatic molecules. In their composite system, thermal fusion of the molecules with rGO during pyrolysis resulted in a highly graphitic material with conductivity as high as 1314 S cm^{-1}.[65] In films, despite the presence of sheet-to-sheet junctions, R_s can fall well below that of individual monolayer since the rGO layers are equivalent to "parallel resistors".[113] Indeed, R_s can be varied over several orders of magnitude depending on the degree of percolation and film thickness.[42,61]

The changes in the electrical conductivity ($\sigma = (R_s t)^{-1}$ where t is the film thickness) as well as optical transmittance of rGO films using chemical and thermal reduction treatments are shown in Figure 10. Upon exposure to hydrazine monohydrate vapor, the film conductivity immediately increases and reaches a saturation value (~10 S cm^{-1}; Fig. 10a). It should be noted that for thick films ($N \gg 5$), reduction by hydrazine vapor is effective only for the top few layers of the GO films, resulting in a saturation of R_s with increasing film thickness.[42] Additional improvement in conductivity can be achieved by annealing the hydrazine-reduced GO films in Ar/H_2 ambient (Fig. 10b). When GO films are reduced by directly annealing in Ar/H_2 without prior exposure to hydrazine, a relatively high annealing temperature (>500 °C) is required to achieve conductivity comparable to those of films reduced at low temperature by hydrazine. In both cases, the highest conductivity (~550 S cm^{-1}) is achieved at an annealing temperature of 1100 °C. The trends in the conductivity are consistent with the chemical composition evolution, which indicates that high C:O ratios are achieved only at high annealing temperatures. It should be noted that the presence of H_2 in the annealing environment does not have a significant impact on the achieved conductivity (Fig. 10b) and C:O ratios.[179] The conductivity values reported for pyrolyzed few-layer GO films are consistently on the order of ~500 S cm^{-1}, irrespective of the oxidation or deposition methods used.[43,60,61,73] This value is comparable to that of polycrystalline graphite (~10^3 S cm^{-1})[202] but is more than an order of magnitude lower than the in-plane

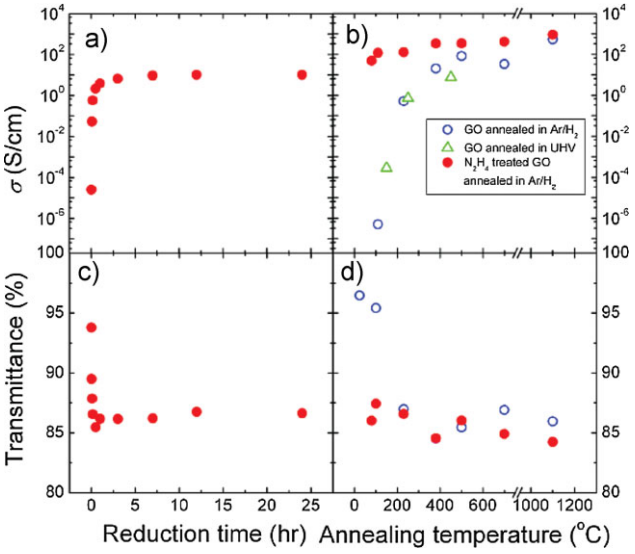

Figure 10. Electrical and optical properties of ~3 layer GO film. a) Conductivity and c) transmittance at $\lambda = 550$ nm of GO film as a function of exposure time to hydrazine monohydrate vapor at 80 °C. b) Conductivity and d) transmittance at $\lambda = 550$ nm of GO reduced with hydrazine monohydrate vapor for 24 h at 80 °C after annealing at different temperatures in Ar/H_2 (solid circle) and that of pristine GO after annealing in Ar/H_2 (open circle) and in UHV (triangles). Reproduced from [43].

conductivity of HOPG (~10^4 S cm^{-1}).[203] It is also worth noting that similar conductivity has been achieved in graphene-like films obtained by pyrolysis of thin photoresist layers.[204]

4.3. Transparent and Conducting Properties

Transparent and conducting electrodes for optoelectronic devices is one of the most anticipated applications of graphene given its extraordinary conductivity and atomic thickness.[25] An ideal sheet of graphene exhibits R_s of ~6 kΩ sq^{-1} with nearly constant optical transparency of ~98% in the visible-IR range.[24] While 6 kΩ sq^{-1} is too large for typical opto-electronic devices, R_s as low as a few hundred Ω sq^{-1}, which is satisfactory for many transparent conductor applications, can be reached by doping.[22] These values compare well with commercially used metal oxide films such as indium tin oxide (ITO) which exhibit R_s of <100 Ω sq^{-1} at ~90% transmittance. Graphene offers several advantages over traditional metal oxide films, especially in the emerging field of flexible, bendable, and stretchable electronics due to its mechanical robustness. The uniform light transmission and chemical stability are also attractive features.[205] Transparent and conducting electrodes made from rGO additionally offer advantages in cost and processability over ITO, which is made from increasingly expensive and scarce indium[206] and requires costly vacuum equipment for deposition.

The first attempt to evaluate rGO as a transparent and conducting material was made for rGO-silica composite thin films.[44] The conductivity was moderate in these films (<1 S cm^{-1}), probably owing to the limited percolation of rGO within the insulating matrix. Wang et al.[60] later demonstrated

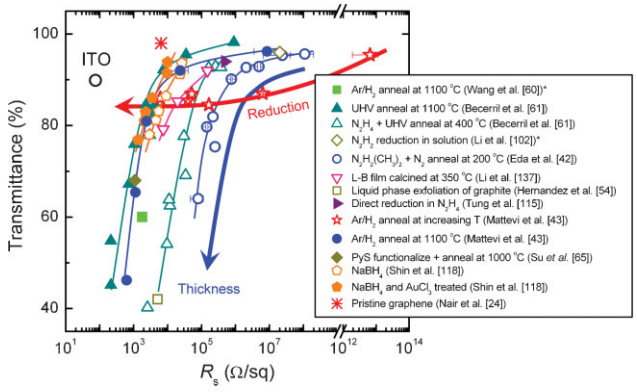

Figure 11. Transmittance at $\lambda = 550$ nm as a function of sheet resistance of rGO films reported by various groups in the literature. In some cases, indicated by (*), the properties were estimated from the information provided. The stars represent the values for the same film thickness annealed at different temperatures. The asterisk in the plot corresponds to the values for ideal grapheme, whose transmittance and sheet resistance are 98%[24] and 6.45 kΩ,[7] respectively.

that thin films of rGO can be made transparent and conducting by optimizing the thickness and reducing at high temperatures. Researchers have employed various oxidation, exfoliation, dispersion, deposition, and reduction procedures, and thus a range of transmittance and sheet resistance values have been reported in the literature, as summarized in Figure 11. The plot shows that the transmittance and sheet resistance decrease with reduction and the overall film thickness. Similar trends indicated by the bold arrows (Fig. 11) are observed in all reports. Efficient reduction is the key to achieving highly conductive films, while the ability to controllably deposit films with nanometer thickness allows high optical transparencies. Currently, the highest degree of reduction is achieved via pyrolysis at 1100 °C, yielding films with the best properties. R_s as low as few kΩ sq^{-1} has been achieved with transmittance of 90% with high temperature pyrolysis. Such sheet resistance values are approximately one order of magnitude higher than those achieved with SWNT network thin films at similar transmittance values.[207]

In order for rGO films to be competitive with other solution-processed alternatives to ITO such as SWNT[207] and metal nanowire[208] thin films that can be deposited at room temperature and used on plastic platforms, high-temperature reduction must be avoided. Direct exfoliation and reduction of GO in hydrazine is a room-temperature route for producing highly reduced GO but yields films with moderate optoelectronic properties[209] (Fig. 11). In addition, use of highly toxic hydrazine requires extreme caution. Efforts in achieving efficient reduction of GO via less hazardous routes at room temperature and doping have provided promising prospects.[62,83,118,123,128] It should be noted that, rather surprisingly, graphene thin films produced via direct exfoliation of graphite in organic solvents[54,55,57] yield values that are comparable to or worse than those of well-reduced GO. The small size of graphene flakes obtained via this route is most likely responsible for the moderate conductivity.

To translate the transparent and conducting properties into optoelectronic devices, several groups have demonstrated the use of rGO thin films as window electrodes for photovoltaic[60,62,63,65,66] and light-emitting[210] devices. Efficient collection of carriers in solar cells and carrier injection in light-emitting diodes (LEDs) depend on appropriate band alignment of each component of the device and the electrical resistance of carrier transport layers. Since the calculated work function of graphene (4.42 eV)[211] nearly coincides with that of ITO (4.4–4.5 eV),[212] replacement of ITO with graphene obviates the need for re-designing the commonly studied photovoltaic or LED structures. With UV photoelectron spectroscopy (UPS), the work function of rGO has been found to increase gradually from 4.2 to 4.4 eV with the C:O ratio.[118] The device-structure and energy-band diagrams of a dye-sensitized solar cell (DSSC) with rGO as the transparent electrode are shown in Figure 12a and 12b, respectively.[60] As the dye absorbs sun light and becomes excited, the electrons are injected into the conduction band of TiO_2 and transported to the rGO electrode. Similarly, holes are transported through the hole-transport layer (denoted as spiro-OMeTAD in Fig. 12b) and collected by the Au cathode. The $I-V$ characteristics of a rGO-based device and a control device with a fluorine tin oxide (FTO) electrode under illumination of simulated sun light are shown in Figure 12c. The comparatively lower short-circuit current (I_{sc}) of the rGO device is attributed to the higher sheet resistance and lower transmittance of rGO compared to those of FTO. The power conversion efficiency is therefore found to be correspondingly lower for the rGO-based device.

Similar results have been reported for organic photovoltaic (OPV) devices with rGO electrodes.[62,63] In commonly studied bulk-heterojunction OPVs based on P3HT-PCBM [poly(hexyl) thiophene-[6-6]phenyl-C_{61}-butyric acid methyl ester mixture] nanocomposites (Fig. 12d), holes (rather than electrons in the case of DSSC) are collected by the window electrode.[213] The rGO-based devices exhibit nearly linear $I-V$ characteristics due to the dominating series resistance of rGO and small shunt resistance giving rise to large reverse bias current (Fig. 12e). It is interesting to note that the short-circuit current and the conversion efficiency of rGO-based devices are found to be less severely influenced by the large sheet resistance of rGO films (approximately three orders of magnitude larger than that of ITO in these demonstrations) than otherwise expected from simple series resistance calculations. These findings point to the importance of investigating the rGO-organic interfacial effects.[73]

4.4. Electric-Field Effect

One of the well-known signatures of graphene and few-layer graphene is the electric-field-dependent transport which, along with the extraordinary carrier mobility, makes them attractive as the channel material for high-frequency field effect transistors.[214] It has been shown that thin films of rGO exhibit a graphene-like ambipoloar field effect when films are made sufficiently thin.[62] Figure 13a shows the schematic of a bottom-gated field effect device with rGO thin film as the channel material. The conductance of the channel between the source (S) and the drain (D) electrodes is modulated by a capacitively coupled gate (G) bias. It should be noted that in rGO thin-film devices, individual rGO sheets typically do not span the source and drain electrodes (Fig. 13b), thereby requiring carriers

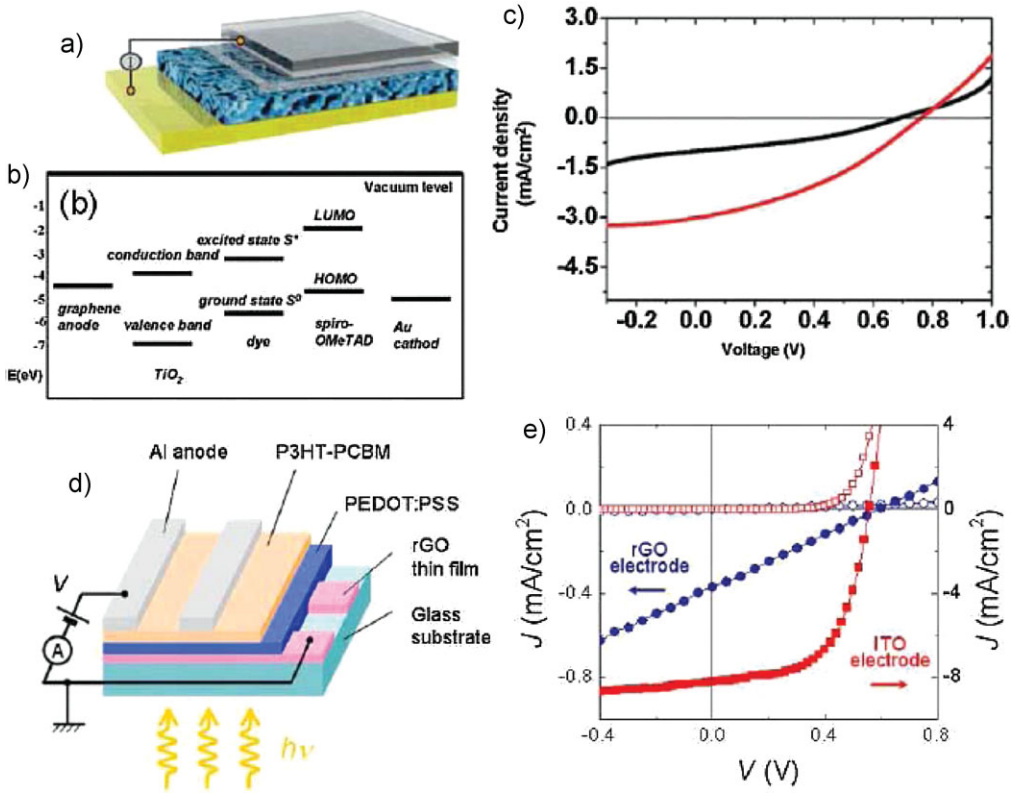

Figure 12. a) Schematic illustration of DSSC using rGO as the window electrode. b) The energy level diagram of DSSC consisting of rGO/TiO_2/dye/spiro-OMeTAD/Au layers. c) *I*–*V* characteristics of rGO-based (black) and FTO-based (red) DSSC under simulated solar illumination. Reproduced with permission from [60]. Copyright 2007, American Chemical Society. d) Structure of OPV having rGO film as the electrode. e) *I*–*V* characteristics of rGO-based (blue) and ITO-based (red) OPV in the dark and under simulated solar illumination (data from Ref. [62] and unpublished work).

to travel from one sheet to another during transport across the channel. Transfer characteristics of ~1.5- and ~4-layer rGO thin-film devices measured at different temperatures are shown in Figure 13c and 13d, respectively. Both devices are ambipoloar, that is, both electron and hole currents can be induced by gate bias. The ''V'' shape of the transfer characteristics is more pronounced for the low temperature measurements of the ~1.5-layer film and the neutrality point, at which the channel conductance reaches minimum, is clearly observed. The characteristic difference between the thin and thick films is the on/off ratio, which is defined as the ratio between the maximum to minimum conductance, G_{max}/G_{min}. Normalized transfer characteristics of ~1.5, ~2.5, and ~4 layer rGO films at $T = 4.2$ K indicates that the field effect diminishes with increasing number of layers (Fig. 13e). This observation is consistent with the fact that a monolayer of graphene is a zero-bandgap semiconductor, while a multilayer graphene is a semimetal.[188] In other words, the DOS at the neutrality point is greater for thicker films, making it difficult to turn off the devices, as is the case for mesoscopic graphite.[215] Similar effects have also been observed for mechanically exfoliated graphene devices.[216] The thickness-dependent temperature dependence of the conductivity reflects this transition.[143] The differences in the on/off ratio, however, are relatively small in mono- to few layer rGO films and are less pronounced at room temperatures (Fig. 13f). The contact resistance of rGO devices is negligible compared to the channel resistance and that field effect in rGO is not a consequence of contact resistance modulation,[217] as is the case in some SWNT-based FETs.[218,219] The on/off ratio of rGO-based devices is typically low (<10), suggesting the presence of defect-related mid-gap states.[220]

Field effect mobilities (μ) can be extracted from the transfer characteristics by:

$$\mu = \frac{L}{WC_{ox}V_{sd}}\frac{\Delta I_{sd}}{\Delta V_g} \quad (1)$$

where L and W are the channel length and the width, respectively, V_{sd} is the source–drain voltage, I_{sd} is the source–drain current, and V_g is the gate voltage. C_{ox} is the gate oxide capacitance and is obtained by $\varepsilon_{ox}\varepsilon_0/t_{ox}$ where ε_{ox} is the permittivity of the oxide, ε_0 is the permittivity of free space, and t_{ox} is the oxide thickness. $\Delta I_{sd}/\Delta V_g$ is the transconductance or the slope of the transfer curve in the linear regime. Field-effect mobilities are obtained from the electron and hole branches of the transfer characteristics. Equation (1) is commonly used in many studies; however, it does not take into account the actual area of percolating conductive paths and therefore underestimates the intrinsic mobility values. Correction factors may be applied based on the

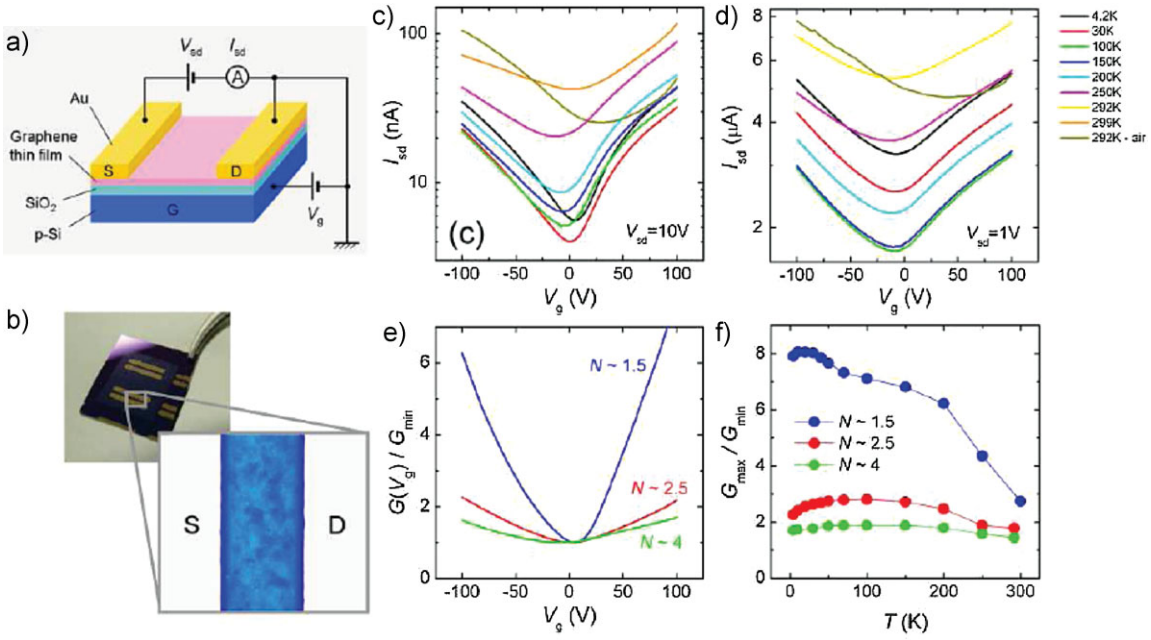

Figure 13. a) Schematic image of rGO TFT. b) Photograph of a rGO TFT with an optical microscopy image showing the S–D region of the device. The channel ($W = 21\,\mu m$) consists of several rGO sheets percolating across the electrodes. c,d) Transfer characteristics of c) ~1.5- and d) ~4-layer films measured at different temperatures. Measurements were conducted in vacuum unless otherwise noted. Reproduced with permission from [42]. Copyright 2008, Nature Publishing Group. e) Normalized channel conductance as a function of gate voltage for ~1.5, ~2.5, and ~4 layer rGO film at $T = 4.2$ K. The channel conductance ($G(V_g)$) is normalized to its minimum value (G_{min}), which occurs at the charge neutrality point.[143] f) on/off ratio, G_{max}/G_{min}, as a function of temperature for ~1.5, ~2.5, and ~4 layer rGO films.[143]

film coverage and the sp^2 carbon fraction.[221] While mobility of up to 365 $cm^2\ V^{-1}\ s^{-1}$ has been reported for well-reduced few-layered films,[183] typical values range between 0.001 and 10 $cm^2\ V^{-1}\ s^{-1}$, depending largely on film thickness and reduction conditions.[42] These values are several orders of magnitude lower than those of mechanically exfoliated graphene (~40 000 $cm^2\ V^{-1}\ s^{-1}$ measured under similar conditions[222]), indicating that residual oxygen and defects in the structure severely limit the carrier transport in rGO. Besides the intrinsic structural defects, substrate-induced charged impurities[223] and contact-induced electron–hole asymmetry[224] are expected to be the limiting factors for mobility.[183] The electron mobilities are generally lower than the hole mobilities at ambient conditions, but the trend is reversed in vacuum, suggesting that adsorbed species may facilitate or limit carrier transport.

Transport studies on individual sheets of rGO provide valuable information since sheet junctions effects can be excluded.[113,114,138,183,185,217,225,226] To fabricate single-rGO devices, individual sheets of GO are deposited onto substrates with prepatterned alignment marks, identified under a microscope, and contacted by metal electrodes following standard lithographic procedures. The transfer characteristics of an individual rGO device with different degrees of reduction are shown in Figure 14a (see figure caption for details). The ambipolar characteristics of well-reduced individual GO devices are in qualitative agreement with those of thin-film counterparts. Typical mobility values also nearly coincide with those of thin-film devices suggesting that sheet junctions in films play a minor role in carrier transport. Figure 14a clearly shows that transport properties of rGO evolve significantly with reduction treatment as GO transforms from insulator to semiconductor to graphene-like semimetal.[217] Lightly reduced GO possesses a finite energy gap and exhibits pronounced switching behavior. Consequently, these samples exhibit insulating off-states with on/off ratio exceeding 10^3 at low temperatures.[217] Upon progressive reduction, rGO approaches the zero-gap limit, leading to a suppressed on/off ratio, while the field-effect mobility improves with increasing sp^2 fraction.

In a similar manner, the transport properties of GO can also be tailored by varying the degree of oxidation during synthesis.[201] Jin et al.[196] recently indicated that the energy gap of GO can be tuned by adjusting the oxidation time. By minimizing the oxidation time, semiconducting GO was obtained without the need for reduction.[201] There are no apparent differences in the device characteristics between those fabricated by controlled oxidation and those obtained by reduction.

4.5. Electrical Conduction Mechanisms

Kaiser et al.[227] reported that electrical conduction in rGO can be described by variable-range hopping (VRH) in 2D materials. In VRH, the temperature dependence of the conductivitym σ is of the form[228]

$$\sigma = \sigma_0 \exp\left(-\frac{B}{T^{1/3}}\right) \quad (2)$$

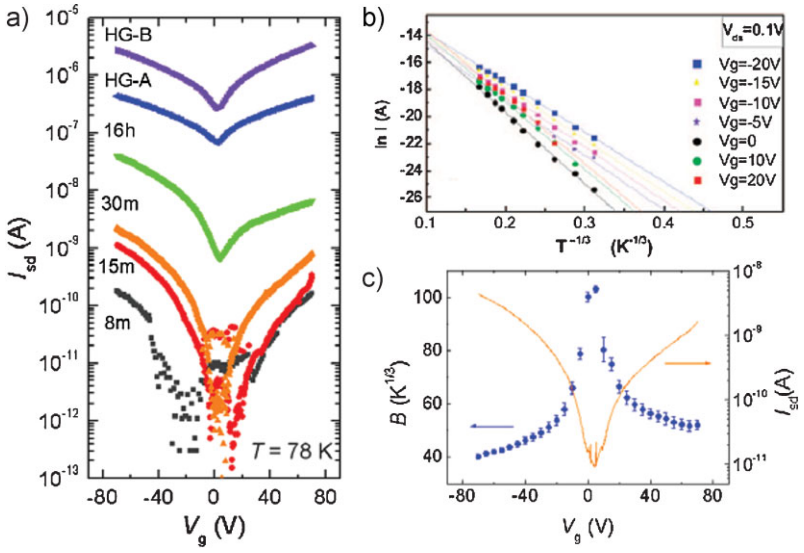

Figure 14. a) Transfer characteristics of a single rGO sheet with different degrees of reduction measured at $T = 78$ K. The labels, 8m, 15m, 30m, and 16h (m = minutes, h = hours) correspond to total time of exposure to hydrazine monohydrate vapor. HG-A and HG-B correspond to GO directly reduced in anhydrous hydrazine with subsequent annealing in forming gas at 150 °C. Reproduced with permission from [217]. Copyright 2009, American Chemical Society. b) ln(I) as a function of $T^{-1/3}$ at different gate voltages showing a fit to 2D VRH model. Reproduced with permission from [227]. Copyright 2009, American Chemical Society. c) Hopping parameter (B) and device current at 100 K (I_{sd}) as a function of gate voltage (unpublished data from Ref. [217]).

The hopping parameter B is expressed as

$$B = \left(\frac{3\alpha^2}{N(E_F)k_B}\right)^{1/3}$$

where α is the wavefunction decay constant, $N(E_F)$ is the DOS at the Fermi level, and k_B is the Boltzmann constant. The temperature dependence of the two-terminal current at fixed V_{sd} and V_g can be fitted well with Equation (2) as shown in Figure 14b. The slope of the linear plot corresponding to the hopping parameter $-B^{1/3}$ changes with V_g, indicating that the gate bias alters the hopping condition rather than simply inducing charges. Further analysis of $B^{1/3}$ as a function of V_g indicates that the hopping condition is most severe near the charge neutrality point, while hopping is facilitated at increased $|V_g|$ (Fig. 14c). These observations are also consistent with the carrier-transport mechanisms in partially hydrogenated graphene.[23]

The evolution of the electronic structure during reduction is indicated by the fact the apparent activation energies associated with carrier concentration (n) and carrier mobility (μ) decrease with the extent of reduction.[217] Particularly, the apparent energy gap of GO gradually approaches zero with reduction. These changes are also seen in the hopping parameter B, which is linked to the electronic DOS and the electronic wave functions of localized states. By examining the hopping parameters and apparent activation energies, localization length ($L_l = 1/\alpha$) of electronic wave functions and $N(E_F)$ can be estimated.[217] Analysis indicates that upon progressive reduction, L_l remains nearly constant while $N(E_F)$ increases by approximately three orders of magnitude. That is, reduction of GO does not lead to delocalization of carriers but to an increased number of localized states near E_F. Indeed, local disorder in graphene such as that present in rGO is expected to give rise to mid-gap energy states.[229] This result is consistent with the fact that the coherence length L_c obtained via Raman spectroscopy remains nearly constant, independent of the extent of reduction.[113]

Studies also show that when GO is minimally defective or extensively reduced, transport is no longer mediated by localized states and show Arrehenius-type temperature dependence. In such cases, fits to VRH model provide unphysical parameters for L_l and bandlike transport is observed.[221,230] The temperature at which the cross-over from VRH to activated transport occurs decreases with the extent of reduction.[217] When VRH conduction dominates the transport, devices typically exhibit strong hysteresis with a gate bias sweep due to charge trapping and transverse-field-dependent mobility.[217,231] These characteristics are not observed in well-reduced samples exhibiting Arrehenius-type temperature dependence.[221]

4.5.1. Percolation Transport

Carriers traveling across rGO thin films are scattered or trapped by sp^3 carbon sites, defects, sheet junctions, and other structural imperfections and impurities. To elucidate the mechanisms limiting the electronic transport properties of rGO films, Mattevi et al.[43] investigated the role of residual oxygen and sp^2 carbon fraction on the electrical conductivity of rGO. Figure 15 shows the plot of conductivity of rGO film under unintentional ambient doping as a function of sp^2-carbon fraction obtained by XPS. The plot also shows data for 100% sp^2-bonded materials (graphene and polycrystalline graphite) for comparison. Extrapolation of the experimental data suggests that it should be possible to achieve conductivity of polycrystalline graphite (1.25×10^3 S cm^{-1})[202] at a sp^2 fraction of ~0.87 in reduced GO. The conductivity corresponding to the minimum conductivity of monolayer graphene (~6×10^3 S cm^{-1})[7] may be achieved by further increasing the sp^2 fraction to >0.9.

The structural model presented in the inset of Figure 15 provides the essential features of transport through rGO at different stages of reduction. Prior to reduction, sp^2 clusters are isolated by oxygen atoms (indicated by dots), rendering GO insulating. As reduction restores sp^2 carbon in GO, the transport barrier between the clusters narrows and allows small fraction of carriers to hop or tunnel among sp^2 sites. Further reduction leads to a greater connectivity among the original sp^2 domains by formation of new, smaller sp^2 clusters with concurrent formation of structural defects due to loss of carbon. Thus, transport at initial stages of reduction occurs via tunneling or hopping among the sp^2 clusters, as indicated by the exponential fit of the data in Figure 14, at low sp^2 fractions (<0.6). At higher sp^2 fractions, percolation among the sp^2 clusters dominates the transport. From the fit, percolation is found to occur at sp^2 fraction of 0.6, which is

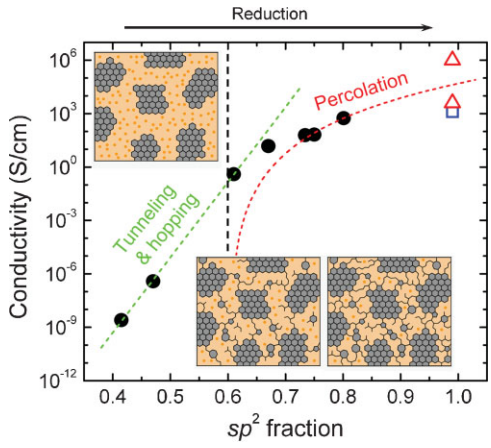

Figure 15. Conductivity of thermally reduced GO as a function of sp^2 carbon fraction obtained from XPS. The vertical dashed line indicates the percolation threshold at sp^2 fraction of ~0.6. Fit to the experimental data reveals two different regimes for electrical transport. Tunneling and/or hopping (green dashed line) dominate the transport at sp^2 fractions below 0.6, while percolation amongst the sp^2 clusters dominates above the percolation threshold. The conductivity values for ~100% sp^2 carbon materials, namely polycrystalline (PC) graphite and graphene, are given for comparison. The two values of graphene correspond to the minimum conductivity (lower triangle) and doped conductivity of ideal graphene with a mobility of 200 000 $cm^2 V^{-1} s^{-1}$ and a carrier density of 10^{12} cm^{-2} (upper triangle), respectively. The inset shows a structural model of GO at different stages of reduction. The gray regions represent sp^2 carbon clusters and the lighter regions represent an sp^3-carbon-rich phase, highly populated with oxygen function groups (dots). With increasing sp^2 fraction (from left to right), the interconnectivity of the sp^2 clusters improves. Reproduced from [43].

in reasonable agreement with the theoretical threshold values for conduction among 2D disks.[232] However, considering the fact that the sp^2 domains are likely to be present in various shapes and sizes and that the nature of sheet-to-sheet junctions are not understood in detail, the percolation conduction model requires further refinement.

4.6. Doping Effect

Owing to its semiconductor-like nature, rGO can be doped under appropriate conditions to achieve appreciable improvements in conductivity. Doping can occur by chemisorption or physisorption of molecules,[22,41,65,177,233] ions,[223] functional groups,[234] metals particles,[235] or ionic liquid.[236] The transfer characteristics resulting from unintentional doping effects from oxygen and water vapor in the ambient are shown in Figure 16a. As-prepared rGO thin films typically exhibit p-type behavior under ambient conditions and threshold voltage (V_{th}) is a large positive value, at which the conductivity minimum is a large positive value (>60 V). The adsorbed and/or trapped water molecules can be partially removed by placing the film in a vacuum dessicator for ~1 week.[143] Subsequent measurements on the same device in ambient conditions with similar relative humidity show a negative shift in V_{th}. It is interesting to note that removal of water vapor also leads to a sharper turn-on behavior of the device with lower G_{min} and improved G_{max}. The field-effect mobility also improves by a factor of ~2 with this treatment.[143] This effect is similar to that of charged impurities in mechanically exfoliated graphene, which severely limit the device mobility.[223,237] When rGO thin films are placed in vacuum, a further negative shift of V_{th} occurs and the ambipolar characteristics become nearly symmetric with V_{th} close to 0 V. This effect can be explained by desorption of oxygen leading to intrinsic behavior, similar to that commonly observed in SWNT-based devices.[238] When the sample is exposed back to ambient air, V_{th} immediately shifts back to positive values (not shown for clarity). Interestingly, the hole mobility decreases slightly, while electron mobility increases with oxygen desorption. This trend is opposite of what is observed in mechanically exfoliated graphene.[223,237] This effect is particularly prominent for low-mobility samples where VRH is the dominant conduction mechanism, suggesting that the adsorbed oxygen gives rise to an increased density of available hopping sites, thereby improving the hopping probability and consequently the carrier mobility.

Studies also show that in some cases, water and oxygen adsorption leads to a decrease in electrical conductivity.[41,186,231] This discrepancy points to the fact that there are few competing effects determining the outcome of doping in rGO. For example, adsorption or chemisorption of molecules may give rise to an increased concentration of one carrier type or compensation of existing carriers. Furthermore, adsorbed or chemisorbed molecules may improve carrier mobility by facilitating hopping or limit mobility by acting as scattering centers as discussed above.

While ambient doping is unintentional, deliberate doping, which is stable in both air and vacuum can also be achieved. For example, simply immersing rGO films in thionyl chloride ($SOCl_2$) or gold chloride ($AuCl_3$) leads to improvement of film conductivity by a factor of 3–5 due to p-type doping by the strongly electronegative chlorine.[62,118] Similar effects have been previously observed for SWNT thin films.[239,240] The mechanism for Cl attachment to rGO is likely to be comparable to the SWNT case, where nucleophilic substitution of OH groups with Cl takes place.[239] The transfer characteristics of the rGO device before and after $SOCl_2$ treatment reveal that, unlike the case of oxygen doping, the effect of Cl doping, as indicated by the positive shift of V_{th}, persists in vacuum suggesting a stable attachment of Cl (Fig. 16b). Measurements at $T = 4.2$ K show that Cl doping leads to asymmetry in the ambipolar characteristics (Fig. 16c). The asymmetry is a manifestation of the fact that the hole mobility improves by a factor of 5 with Cl doping, while the electron mobility remains almost unchanged. As discussed above for the case of oxygen doping, the dopant acceptor states are expected to facilitate hopping conduction. This type of doping allows improvement of film conductivity without degrading the film transparency.[239] An appropriate choice of doping would therefore be a key for realizing high-performance rGO-based transparent conductors. Further, breaking the symmetry of ambipolar characteristics via doping offers a route for converting an ambipolar device to a unipolar one.

It is known that adsorbed hydrazine as well as C–N groups in carbon-based materials act as donors.[241,242] However, despite the

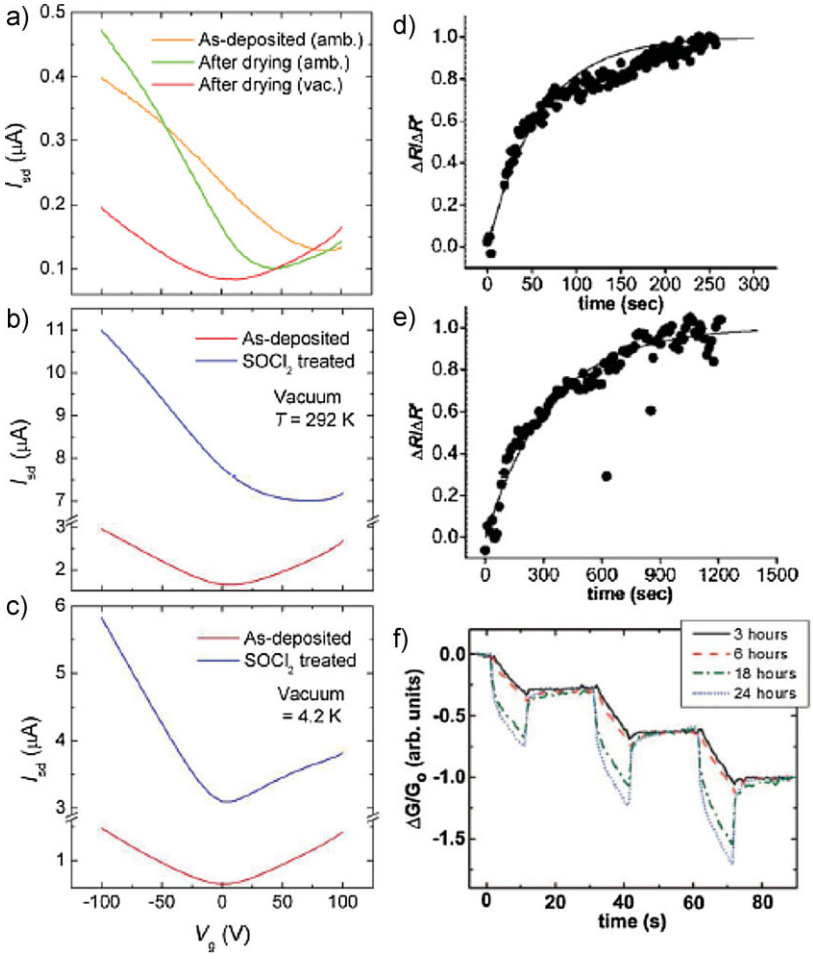

Figure 16. a) Transfer characteristics of a rGO film device before and after drying, measured in ambient conditions and subsequently in vacuum [143]. b,c) Transfer characteristics of a rGO film device before and after $SOCl_2$ treatment measured in vacuum at room temperature (b)and at 4.2 K (c). Reproduced with permission from [42]. Copyright 2008, Nature Publishing Group. Normalized resistance change ($\Delta R/\Delta R'$, where ΔR is the change of resistance and $\Delta R'$ is the resistance change at the saturated state) as a function of time of exposure to water vapor at base pressure of $\sim 10^{-5}$ Torr for thermally reduced GO (d) and for a chemically and thermally reduced GO (e). Reproduced with permission from [231]. Copyright 2008, American Chemical Society. f) Normalized conductance change ($\Delta G/G_0$) to 5 s pulses of acetone of increasing concentration for a rGO film reduced with hydrazine for different times. The recoverable conductance increases with increasing reduction time. Reproduced with permission from [41]. Copyright 2008, American Chemical Society.

common use of hydrazine, negative threshold voltage has not been observed in rGO.[217] It is suggested that the activated electrons from such donors are compensated by holes.[118] Intentional n-type doping has been recently reported for GO annealed in NH_3 atmosphere.[126] Li et al.[126] observed simultaneous reduction of GO and incorporation of N atoms into the structure at doping levels of up to ~5%. The C–N formation relies on the reaction between NH_3 and oxygen functional groups of GO such as carboxyl, carbonyl, and lactone groups. N-doped rGO field-effect devices exhibit negative V_{th}, improved conductivity, and suppressed on/off behavior compared to pristine rGO.[126]

4.7. Sensors Based on rGO

High sensitivity of rGO to gases and vapors form the basis of realizing rGO molecular sensors. Studies show that resistance (or conductance) of rGO increases (or decreases) upon exposure to a wide variety of chemical species, including potential warfare agents at ppb concentrations.[41] Molecules may bind to structural defects in rGO such as vacancies and functional groups or graphitic sp^2 domains.[243] The binding energies of molecules to attach onto rGO largely depend on the type and density of available sites.[243] Since reduction history determines the density of residual oxygen functional groups, the detection sensitivity of rGO-based sensors can be potentially tailored by carefully designing the reduction treatment.[41,231] Figure 16d and 16e show normalized resistance response to water vapor at a constant pressure for two rGO devices; one reduced thermally and the other reduced via a combination of chemical and thermal reduction, respectively. Jung et al.[231] have indicated that the delayed response in the latter device can be explained by lower concentration of defects that can act as strong binding sites and the presence of C–N groups (due to hydrazine treatment), which bind weakly with water in comparison to C–O groups.

Molecules that are weakly adsorbed onto rGO via dispersive forces can desorb with thermal energy at room temperature. Conductance changes associated with weakly bound molecules are therefore recoverable upon evacuation.[41] On the other hand, strongly bound molecules induce conductance changes, which are non-recoverable unless mildly heated.[41] Graphitic sp^2 domains act as weak binding sites, whereas vacancies and oxygen functional groups can form stronger physical bonds, particularly with polar molecules.[243] Conductance changes associated with molecular adsorption therefore consists of recoverable and non-recoverable portions. Robinson et al.[41] demonstrated that in contrast to sensors based on SWNTs, rGO-based sensors exhibit only moderately recoverable conductance changes, consistent with the presence of appreciable concentration of defects and residual oxygen groups. Further, controlled reduction allows tailoring of recoverable and non-recoverable response, as shown in Figure 16f. It is also worth noting that layered rGO film structure leads to appreciable suppression of $1/f$ noise due to charged impurity screening[244] giving rise to large signal-to-noise ratios.[41]

4.8. Composite Thin-Film Devices

Incorporation of rGO sheets into polymer[34,245–247] or ceramic[44] matrices have been demonstrated to exhibit remarkable

improvements in the physical properties of the host material. For example, the mechanical and thermal properties of rGO-based polymer composites rank among the best in comparison with other carbon-based composites.[248] This is enabled by strong interactions between polymer hosts and graphene sheets[246,248] and the very large aspect ratio of rGO sheets, which allows percolation at low loadings (~0.1 vol%).[34] Ease of dispersion and exceptionally low percolation threshold make rGO composites attractive for a range of applications. While initial studies have focused on the conventional properties of composites, recent reports have indicated possibilities for thin-film electronic and optoelectronic applications. In this Section, some recent studies on rGO-polymer composite devices are briefly reviewed.

Fabrication of rGO-polymer composite generally requires GO sheets to be functionalized, such that they are soluble in solvents that are compatible with host polymers. Other routes obviating the need for additional functionalization steps are also available.[249] Functionalization of GO with aryl and alkyl isocyanates, as proposed by Stankovich et al.[93] allows dissolution of GO in polar aprotic solvents such as dimethylformamide (DMF) and *N*-methylpyrrolidone (NMP), which are common solvents for dissolving many polymers. Isocyanates react with hydroxyl and carboxyl groups in GO to form carbamate and amide groups, respectively, while the epoxy groups remain unreacted.[93] Functionalized GO can be chemically reduced in organic solvents prior to deposition to achieve rGO-polymer solution. Composite thin films can be obtained via spin-coating such solution, followed by mild annealing to drive off residual solvents and reducing chemicals.

In contrast to hot-pressed bulk composite samples, in which rGO sheets are randomly oriented,[34,248] the orientation of rGO sheets in thin films can be varied from random to lateral orientation by simply controlling the spin-coating speeds during deposition.[75] At low spin-coating speeds, the shear force is sufficiently low to maintain the random orientation of rGO sheets and the polymer solidifies before the sheets align parallel to the substrate surface as schematically described in Figure 17a. Some rGO sheets can protrude from the composite surface at low spin-coating speeds. At high spin-coating speeds, the sheets are sparsely distributed and oriented almost parallel to substrate surface (Fig. 17a). The orientation of rGO sheets determines the preferred charge-transport direction.[75]

4.8.1. Thin-Film Transistors

Introduction of percolating rGO network within an insulating material can render it semiconducting.[72] Figure 17b shows transfer characteristics of a bottom-gated field-effect device consisting of polystyrene (PS) as the host and 10 vol% rGO as the filler material. The ambipolar characteristics are comparable to those of rGO films (Fig. 13c), suggesting that the influence of PS in charge conduction and gate capacitance is minor. The conductivity of these films at $V_g = 0$ V range from 1 to 24 S m^{-1}, in agreement with the values reported for bulk composites.[34] In contrast to rGO films, the field-effect mobility was found to be generally higher for

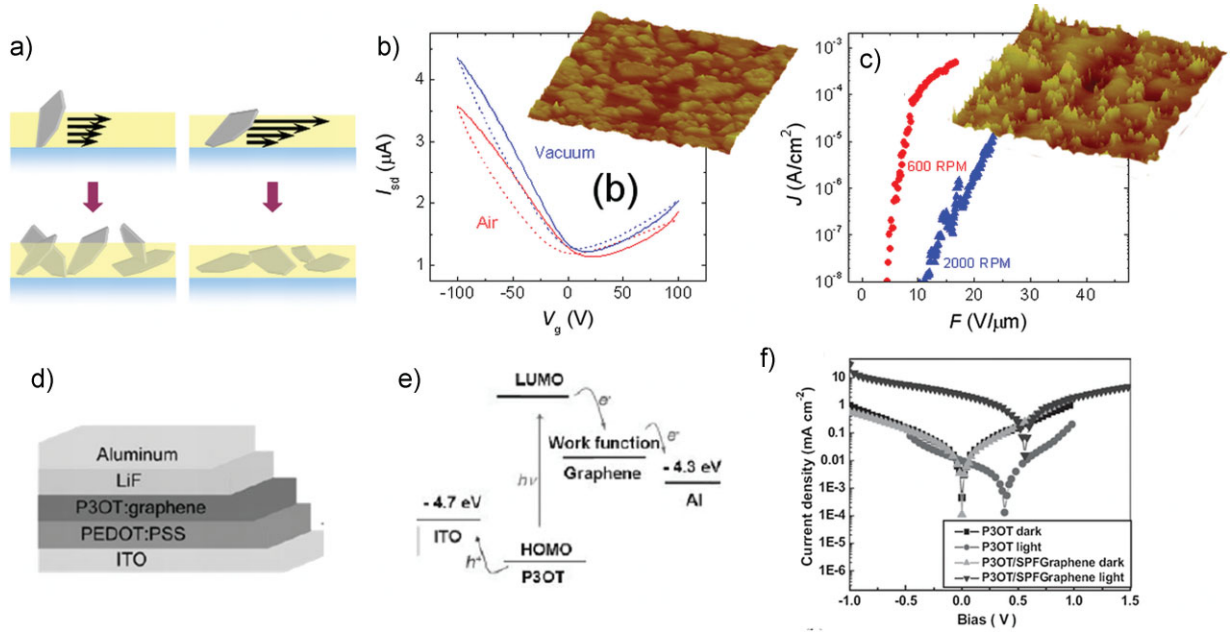

Figure 17. a) Schematic of the spin-coating process of rGO-polymer composite for low (left) and high (right) speeds leading to different sheet orientations. Reproduced with permission from [75]. Copyright 2008, American Institute of Physics. b) Transfer characteristics of rGO-PS composite films in ambient conditions and vacuum. The inset shows an AFM image (10 μm × 10 μm) of the film indicating that rGO sheets lie parallel to the substrate surface. Reproduced with permission from [72]. Copyright 2009, American Chemical Society. c) Field-emission current density (*J*) vs applied field (*F*) for rGO-PS composite films deposited at 600 and 2000 rpm. The inset shows an AFM image (5 μm × 5 μm) of the film indicating that some rGO sheet edges protrude from the surface. Reproduced with permission from [75]. Copyright 2008, American Institute of Physics. d) Schematic of OPV device with rGO as the acceptor material. e) Energy-level diagram of the device showing exciton formation in P3OT, electron transport to Al electrodes via rGO, and hole transport to ITO. f) *I*–*V* characteristics of a OPV devices with and without 5 wt% rGO incorporated into a P3OT layer in the dark and under simulated solar illumination. Reproduced from [77].

holes than for electrons by a factor of 2–5 in vacuum, exhibiting values between 0.1 and 1 $cm^2\ V^{-1}\ s^{-1}$. Unlike rGO films, the composite devices are only weakly sensitive to unintentional ambient doping, suggesting that the majority of rGO responsible for the carrier transport are embedded within the PS (Fig. 16b). Thus, the insulating PS matrix provides structural integrity and air stability, while minimally interfering with the electrical properties of the rGO network.

4.8.2. Field-Emission Devices

Motivated by earlier works on field emission from graphitic flakes dispersed in insulating media,[250,251] it was anticipated that rGO-PS composites would yield improved field enhancement due to atomically sharp edges allowing extraction of electrons into the vacuum at low-threshold electric fields.[252] For efficient field emission, rGO sheets must be oriented vertically and not lie flat on the substrate. As mentioned above, deposition of composite films at low spin-coating speeds allow some rGO sheets to protrude from the composite surface. The field-emission characteristics of two composite films deposited at different spin-coating speeds show that the threshold field required to drive a current density of 10^{-8} A cm^{-2} is significantly lower for the 600 rpm sample (~4 V μm^{-1}) in comparison to the 2000 rpm sample (~11 V μm^{-1}) (Fig. 16c).

The lower threshold field for electron emission in the 600 rpm sample is attributed to the field enhancement near the edges of the rGO sheets that are oriented semivertically to the substrate. Fowler–Nordheim[253] analysis shows that the field-enhancement factor for the 600 rpm sample is 1200, while it is 700 for the 2000 rpm sample. The threshold field for the rGO composite films is higher than the lowest threshold fields of carbon nanotubes[254] and other carbon-based materials[255,256] (0.5–1 V μm^{-1}) reported in the literature. However, the field-emission characteristics of rGO-PS composite films are comparable to those of carbon nanotube–polymer composite field emitters.[257] Although the emission-current stability and spatial uniformity require significant improvement for realistic applications, rGO-based composites are attractive because of their solution processabity, allowing deposition at low temperatures.

4.8.3. Bulk Heterojunction Photovoltaics

Incorporation of rGO into non-insulating polymers also allows the exploration of new functionalities. Liu et al.[77] used rGO as the acceptor material for polymer bulk heterojunction (BHJ) photovoltaic devices (Fig. 17d). Commonly studied polymer BHJ devices consist of P3HT or P3OT (poly(3-octylthiophene)) as the electron-donor and PCBM as the electron-acceptor material. In order for photon energies to be harvested, generated excitons must be dissociated at the heterojunction and transported to electrodes. Large surface-to-volume ratio and relatively high carrier mobility of rGO render it an alternative electron acceptor and transport material for OPV applications. Incorporation of rGO into P3HT or P3OT can be achieved using functionalization schemes similar to those utilized for rGO-PS composites. Liu et al.[77] observed quenching of P3HT photoluminesce after introduction of rGO, suggesting some energy/electron transfer.[77] Photovoltaic devices based on rGO-P3OT and rGO-P3HT systems exhibit power conversion efficiencies of 1.4% and 1.1%, respectively, significantly better than SWNT/P3HT devices.[258] The efficiency values of rGO/P3HT devices also compares very positively with those of inorganic/organic BHJ devices,[259,260] suggesting that there is trememdous promise for such applicatoins if the results of Liu et al. are confirmed. The major challenge with rGO-based BHJ photovoltaic and other optoelectronic and electronic devices is the efficient dispersion of GO with the polymer and reduction without degrading the intrinsic properties of the host material. Dispersion and reduction schemes, which do not require exposure of the host material to reactive chemicals and high temperatures is essential for improving the device performance.

5. Conclusions and Outlook

Chemical exfoliation of graphite, yielding GO, provides a practical route towards low-cost bulk production, ease of deposition, and tunable optoelectronic properties of graphene-based thin films. The chemical versatility of GO is a unique feature of the material that allows solubility in a variety of solvents, incorporation into composites, and tailoring of its properties over a wide range. Solution-based deposition of GO and GO-based composite thin films can be achieved by a variety of methods and allows fabrication of transparent conductors, TFTs, sensors, field emitters, photovoltaics, and memory devices without extensive lithographic processing. Although rGO-based transparent conductors require further work to compete with state-of-the-art materials, the advantages of low-cost and high-through-put deposition make them compelling for niche applications. The carrier mobility of rGO (up to 365 $cm^2\ V^{-1}\ s^{-1}$) is significantly better than that of existing conjugated polymers and amorphous silicon, making it attractive for macroscale electronics.[261] However, the switching behavior must be significantly improved if logic devices are to be realized with rGO. In this respect, a chemical route for tuning the energy gap of GO/rGO remains a major challenge.

The PL properties of GO and its derivatives are only beginning to be revealed. Recent observation of blue PL from GO[192,195] opens up exciting opportunities for exploration of photonic devices such as electroluminescent cells, photodetectors, and photovoltaics. Molecular sensing with rGO is highly promising due to large signal-to-noise ratio and extremely high sensitivity to certain chemicals. For practical applications, selectivity to specific molecules and stability against repeated adsorption and desorption cycles require closer examination. The compatibility of rGO with polymers and ceramics opens up a route for realization of functional composite materials[262] from electrically passive and active host materials. This field is only emerging but merging of GO-based materials with organic[70,72,75–78,249,263,264] or inorganic[44,131,265–270] materials should continue to present numerous new and exciting possibilities.

While the degree of oxidation and reduction can be used as the knob to broadly tune the properties of GO and rGO films, precise control over the properties require detailed understanding of nanometer- to sub-nanometer-scale structure of the material. Properties of GO and rGO films are not uniquely determined by the C:O ratio or sp^2 carbon fraction but are strongly influenced by the distribution of sp^2 carbon and structural defects such as

vacancies. The sp^2 carbon in GO forms non-percolating clusters, where confinement of electrons results in local energy gaps. Since energy gaps allow PL to occur, the implication of sp^2 clusters deserves further attention. For efficient carrier transport, a percolating network of sp^2 carbon is required. The key to improving carrier mobility is to minimize structural defects caused by carbon loss from graphene plane during the synthesis of GO and reduction.[185] Further, effects of macroscopic structural defects such as wrinkles, folds, and sheet junctions on transport properties need to be investigated for device optimization.

Although much progress has been made in understanding the structure, processing, and properties of GO/rGO-based thin films, there is significantly more to be explored and exploited given the highly versatile properties of the material. GO provides an exciting platform to study engineering, physics, chemistry, and materials science of unique 2D systems as well as offers a route towards realizing carbon-based thin-film technology. Continued involvement of researchers from all disciplines should further uncover the potential of GO/rGO in thin film electronics and optoelectronics.

Acknowledgements

This research is funded by the NSF CAREER Award (ECS 0543867). The authors thank the current and former members of the Nanomaterials and Devices group at Rutgers University (Dr. Giovanni Fanchini, Dr. Cecilia Mattevi, Dr. Hisato Yamaguchi, Dr. Steve Miller, Dr. Alokik Kanwal, and HoKwon Kim) and the collaborators who contributed to the original studies (Prof. Chun-Wei Chen at the National Taiwan University, Prof. K. Andre Mkhoyan at the University of Minnesota, Prof. Gehan Amaratunga at the University of Cambridge, Prof. Eric Garfunkel at Rutgers University, and Prof. Gaetano Granozzi at the University of Padova). We also acknowledge the financial support from Center for Advanced Structural Ceramics (CASC) at Imperial College London. G.E. acknowledges the Royal Society for the Newton International Fellowship. M.C. acknowledges support from the Royal Society through the Wolfson Merit Award.

Received: October 28, 2009
Published online: April 28, 2010

[1] H. P. Boehm, A. Clauss, G. O. Fischer, U. Hofmann, *Z. Naturforschung* **1962**, *17b*, 150.
[2] J. W. May, *Surf. Sci.* **1969**, *17*, 267.
[3] H. P. Boehm, R. Setton, E. Stumpp, *Carbon* **1986**, *24*, 241.
[4] X. Lu, M. Yu, H. Huang, R. S. Ruoff, *Nanotechnology* **1999**, *10*, 269.
[5] K. S. Novoselov, A. K. Geim, S. V. Morozov, D. Jiang, Y. Zhang, S. V. Dubonos, I. V. Grigorieva, A. A. Firsov, *Science* **2004**, *306*, 666.
[6] K. S. Novoselov, D. Jiang, F. Schedin, T. J. Booth, V. V. Khotkevich, S. V. Morozov, A. K. Geim, *Proc. Nat. Acad. Sci. U. S. A.* **2005**, *102*, 10451.
[7] K. S. Novoselov, A. K. Geim, S. V. Morozov, D. Jiang, M. I. Katsnelson, I. V. Grigorieva, S. V. Dubonos, A. A. Firsov, *Nature* **2005**, *438*, 197.
[8] Y. B. Zhang, Y. W. Tan, H. L. Stormer, P. Kim, *Nature* **2005**, *438*, 201.
[9] A. K. Geim, K. S. Novoselov, *Nat. Mater.* **2007**, *6*, 183.
[10] A. K. Geim, P. Kim, *Sci. Am.* **2008**, *298*, 68.
[11] S. V. Morozov, K. S. Novoselov, M. I. Katsnelson, F. Schedin, D. C. Elias, J. A. Jaszczak, A. K. Geim, *Phys. Rev. Lett.* **2008**, *100*, 016602.
[12] X. Du, I. Skachko, A. Barker, E. Y. Andrei, *Nat. Nanotechnol.* **2008**, *3*, 491.
[13] K. I. Bolotin, K. J. Sikes, Z. Jiang, G. Fudenberg, J. Hone, P. Kim, H. L. Stormer, *Sol. Stat. Commun.* **2008**, *146*, 351.
[14] F. Miao, S. Wijeratne, Y. Zhang, U. C. Coskun, W. Bao, C. N. Lau, *Science* **2007**, *317*, 1530.
[15] K. S. Novoselov, Z. Jiang, Y. Zhang, S. V. Morozov, H. L. Stormer, U. Zeitler, J. C. Maan, G. S. Boebinger, P. Kim, A. K. Geim, *Science* **2007**, *315*, 1379.
[16] S. Pisana, M. Lazzeri, C. Casiraghi, K. S. Novoselov, A. K. Geim, A. C. Ferrari, F. Mauri, *Nat. Mater.* **2007**, *6*, 198.
[17] D. L. Miller, K. D. Kubista, G. M. Rutter, M. Ruan, W. A. de Heer, P. N. First, J. A. Stroscio, *Science* **2009**, *324*, 924.
[18] M. I. Katsnelson, K. S. Novoselov, A. K. Geim, *Nat. Phys.* **2006**, *2*, 620.
[19] A. F. Young, P. Kim, *Nat. Phys.* **2009**, *5*, 222.
[20] C. Lee, X. Wei, J. W. Kysar, J. Hone, *Science* **2008**, *321*, 385.
[21] A. A. Balandin, S. Ghosh, W. Bao, I. Calizo, D. Teweldebrhan, F. Miao, C. N. Lau, *Nano Lett.* **2008**, *8*, 902.
[22] F. Schedin, A. K. Geim, S. V. Morozov, E. W. Hill, P. Blake, M. I. Katsnelson, K. S. Novoselov, *Nat. Mater.* **2007**, *6*, 652.
[23] D. C. Elias, R. R. Nair, T. M. G. Mohiuddin, S. V. Morozov, P. Blake, M. P. Halsall, A. C. Ferrari, D. W. Boukhvalov, M. I. Katsnelson, A. K. Geim, K. S. Novoselov, *Science* **2009**, *323*, 610.
[24] R. R. Nair, P. Blake, A. N. Grigorenko, K. Novoselov, T. J. Booth, T. Stauber, N. M. R. Peres, A. K. Geim, *Science* **2008**, *320*, 1308.
[25] A. K. Geim, *Science* **2009**, *324*, 1530.
[26] S. Park, R. S. Ruoff, *Nat. Nanotechnol.* **2009**, *4*, 217.
[27] C. N. R. Rao, K. Biswas, K. S. Subrahmanyam, A. Govindaraj, *J. Mater. Chem.* **2009**, *19*, 2457.
[28] C. N. R. Rao, A. K. Sood, K. S. Subrahmanyam, A. Govindaraj, *Angew. Chem. Int. Ed.* **2009**, *48*, 7752.
[29] M. J. Allen, V. C. Tung, R. B. Kaner, *Chem. Rev.* **2009**, *110*, 132.
[30] K. P. Loh, Q. Bao, P. K. Ang, J. Yang, *J. Mater. Chem.* **2010**, DOI: 10.1039/b920539j.
[31] J. Wintterlin, M. L. Bocquet, *Surf. Sci.* **2009**, *603*, 1841.
[32] S. Stankovich, D. A. Dikin, R. D. Piner, K. A. Kohlhaas, A. Kleinhammes, Y. Jia, Y. Wu, S. T. Nguyen, R. S. Ruoff, *Carbon* **2007**, *45*, 1558.
[33] S. Stankovich, R. D. Piner, X. Q. Chen, N. Q. Wu, S. T. Nguyen, R. S. Ruoff, *J. Mater. Chem.* **2006**, *16*, 155.
[34] S. Stankovich, D. A. Dikin, G. H. B. Dommett, K. M. Kohlhaas, E. J. Zimney, E. A. Stach, R. D. Piner, S. T. Nguyen, R. S. Ruoff, *Nature* **2006**, *442*, 282.
[35] H. Hiura, T. W. Ebbesen, J. Fujita, K. Tanigaki, T. Takada, *Nature* **1994**, *367*, 148.
[36] T. W. Ebbesen, H. Hiura, *Adv. Mater.* **1995**, *7*, 582.
[37] K. A. Worsley, P. Ramesh, S. K. Mandal, S. Niyogi, M. E. Itkis, R. C. Haddon, *Chem. Phys. Lett.* **2007**, *445*, 51.
[38] E. Widenkvist, D. W. Boukhvalov, S. Rubino, S. Akhtar, J. Lu, R. A. Quinlan, M. I. Katsnelson, K. Leifer, H. Grennberg, U. Jansson, *J. Phys. D: Appl. Phys.* **2009**, *42*, 112003.
[39] D. A. Dikin, S. Stankovich, E. J. Zimney, R. D. Piner, G. H. B. Dommett, G. Evmenenko, S. T. Nguyen, R. S. Ruoff, *Nature* **2007**, *448*, 457.
[40] J. T. Robinson, M. Zalalutdinov, J. W. Baldwin, E. S. Snow, Z. Wei, P. Sheehan, B. H. Houston, *Nano Lett.* **2008**, *8*, 3441.
[41] J. T. Robinson, F. K. Perkins, E. S. Snow, Z. Wei, P. E. Sheehan, *Nano Lett.* **2008**, *8*, 3137.
[42] G. Eda, G. Fanchini, M. Chhowalla, *Nat. Nanotechnol.* **2008**, *3*, 270.
[43] C. Mattevi, G. Eda, S. Agnoli, S. Miller, K. A. Mkhoyan, O. Celik, D. Mastrogiovanni, G. Granozzi, E. Garfunkel, M. Chhowalla, *Adv. Funct. Mater.* **2009**, *19*, 2577.
[44] S. Watcharotone, D. A. Dikin, S. Stankovich, R. Piner, I. Jung, G. H. B. Dommett, G. Evmenenko, S. E. Wu, S. F. Chen, C. P. Liu, S. T. Nguyen, R. S. Ruoff, *Nano Lett.* **2007**, *7*, 1888.
[45] J. Coraux, A. T. N'Diaye, C. Busse, T. Michely, *Nano Lett.* **2008**, *8*, 565.
[46] P. W. Sutter, J.-I. Flege, E. A. Sutter, *Nat. Mater.* **2008**, *7*, 406.
[47] A. Reina, X. Jia, J. Ho, D. Nezich, H. Son, V. Bulovic, M. S. Dresselhaus, J. Kong, *Nano Lett.* **2009**, *9*, 30.

[48] K. S. Kim, Y. Zhao, H. Jang, S. Y. Lee, J. M. Kim, K. S. Kim, J.-H. Ahn, P. Kim, J.-Y. Choi, B. H. Hong, *Nature* **2009**, *457*, 706.
[49] X. Li, W. Cai, J. An, S. Kim, J. Nah, D. Yang, R. Piner, A. Velamakanni, I. Jung, E. Tutuc, S. K. Banerjee, L. Colombo, R. S. Ruoff, *Science* **2009**, *324*, 1312.
[50] A. J. V. Bommel, J. E. Crombeen, A. V. Tooren, *Surf. Sci.* **1975**, *48*, 463.
[51] C. Berger, Z. M. Song, T. B. Li, X. B. Li, A. Y. Ogbazghi, R. Feng, Z. T. Dai, A. N. Marchenkov, E. H. Conrad, P. N. First, W. A. de Heer, *J. Phys. Chem. B* **2004**, *108*, 19912.
[52] C. Berger, Z. M. Song, X. B. Li, X. S. Wu, N. Brown, C. Naud, D. Mayo, T. B. Li, J. Hass, A. N. Marchenkov, E. H. Conrad, P. N. First, W. A. de Heer, *Science* **2006**, *312*, 1191.
[53] K. V. Emtsev, A. Bostwick, K. Horn, J. Jobst, G. L. Kellogg, L. Ley, J. L. McChesney, T. Ohta, S. A. Reshanov, J. Rohrl, E. Rotenberg, A. K. Schmid, D. Waldmann, H. B. Weber, T. Seyller, *Nat. Mater.* **2009**, *8*, 203.
[54] Y. Hernandez, V. Nicolosi, M. Lotya, F. M. Blighe, Z. Sun, S. De, I. T. McGovern, B. Holland, M. Byrne, Y. K. Gun'Ko, J. J. Boland, P. Niraj, G. Duesberg, S. Krishnamurthy, R. Goodhue, J. Hutchison, V. Scardaci, A. C. Ferrari, J. N. Coleman, *Nat. Nanotechnol.* **2008**, *3*, 563.
[55] S. Biswas, L. T. Drzal, *Nano Lett.* **2008**, *9*, 167.
[56] L. Na, L. Fang, W. Haoxi, L. Yinghui, Z. Chao, C. Ji, *Adv. Funct. Mater.* **2008**, *18*, 1518.
[57] L. Jong Hak, S. Dong Wook. G. M. Victor, S. N. Albert, E. F. Vladimir, K. Yu Hee. C. Jae-Young, K. Jong Min, Y. Ji-Beom, *Adv. Mater.* **2009**, *21*, 1.
[58] M. Lotya, Y. Hernandez, P. J. King, R. J. Smith, V. Nicolosi, L. S. Karlsson, F. M. Blighe, S. De, Z. Wang, I. T. McGovern, G. S. Duesberg, J. N. Coleman, *J. Am. Chem. Soc.* **2009**, *131*, 3611.
[59] Q. Cao, J. Rogers, *Adv. Mater.* **2008**, *20*, 1.
[60] X. Wang, L. Zhi, K. Müllen, *Nano Lett.* **2008**, *8*, 323.
[61] H. A. Becerill, J. Mao, Z. Liu, R. M. Stoltenberg, Z. Bao, Y. Chen, *ACS Nano* **2008**, *2*, 463.
[62] G. Eda, Y.-Y. Lin, S. Miller, C.-W. Chen, W.-F. Su, M. Chhowalla, *Appl. Phys. Lett.* **2008**, *92*, 233305.
[63] J. Wu, H. A. Becerril, Z. Bao, Z. Liu, Y. Chen, P. Peumans, *Appl. Phys. Lett.* **2008**, *92*, 263302.
[64] Y. Zhu, W. Cai, R. D. Piner, A. Velamakanni, R. S. Ruoff, *Appl. Phys. Lett.* **2009**, *95*, 103104.
[65] Q. Su, S. Pang, V. Alijani, C. Li, X. Feng, K. Müllen, *Adv. Mater.* **2009**, *21*, 1.
[66] Z. Yin, S. Wu, X. Zhou, X. Huang, Q. Zhang, F. Boey, H. Zhang, *Small* **2009**, *6*, 307.
[67] R. Arsat, M. Breedon, M. Shafiei, P. G. Spizziri, S. Gilje, R. B. Kaner, K. Kalantar-zadeh, W. Wlodarski, *Chem. Phys. Lett.* **2009**, *467*, 344.
[68] N. Mohanty, V. Berry, *Nano Lett.* **2008**, *8*, 4469.
[69] J. Fowler, M. Allen, V. Tung, Y. Yang, R. Kaner, B. Weiller, *ACS Nano* **2009**, *3*, 301.
[70] L. J. Cote, R. Cruz-Silva, J. Huang, *J. Am. Chem. Soc.* **2009**, *131*, 11027.
[71] M. Zhou, Y. Zhai, S. Dong, *Anal. Chem.* **2009**, *81*, 5603.
[72] G. Eda, M. Chhowalla, *Nano Lett.* **2009**, *9*, 814.
[73] S. Pang, H. N. Tsao, X. Feng, K. Müllen, *Adv. Mater.* **2009**, *21*, 3488.
[74] M. D. Stoller, S. Park, Y. Zhu, J. An, R. S. Ruoff, *Nano Lett.* **2008**, *8*, 3498.
[75] G. Eda, H. E. Unalan, N. Rupesinghe, G. Amaratunga, M. Chhowalla, *Appl. Phys. Lett.* **2008**, *93*, 233502.
[76] Q. Liu, Z. Liu, X. Zhang, N. Zhang, L. Yang, S. Yin, Y. Chen, *Appl. Phys. Lett.* **2008**, *92*, 223303.
[77] Z. Liu, Q. Liu, Y. Huang, Y. Ma, S. Yin, X. Zhang, W. Sun, Y. Chen, *Adv. Mater.* **2008**, *20*, 3924.
[78] Q. Liu, Z. Liu, X. Zhang, L. Yang, N. Zhang, G. Pan, S. Yin, Y. Chen, W. Jun, *Adv. Funct. Mater* **2009**, *19*, 894.
[79] K. K. Manga, Y. Zhou, Y. Yan, K. P. Loh, *Adv. Funct. Mater.* **2009**, *19*, 3638.
[80] X. Lv, Y. Huang, Z. Liu, J. Tian, Y. Wang, Y. Ma, J. Liang, S. Fu, X. Wan, Y. Chen, *Small* **2009**, *5*, 1682.
[81] X.-D. Zhuang, Y. Chen, G. Liu, P.-P. Li, C.-X. Zhu, E.-T. Kang, K.-G. Noeh, B. Zhang, J.-H. Zhu, Y.-X. Li, *Adv. Mater.* in press.
[82] C. L. He, F. Zhuge, X. F. Zhou, M. Li, G. C. Zhou, Y. W. Liu, J. Z. Wang, B. Chen, W. J. Su, Z. P. Liu, Y. H. Wu, P. Cui, L. Run-Wei, *Appl. Phys. Lett.* **2009**, *95*, 232101.
[83] W. Gao, L. B. Alemany, L. Ci, P. M. Ajayan, *Nat. Chem.* **2009**, *1*, 403.
[84] B. C. Brodie, *Philos. Trans. R. Soc. London* **1959**, *149*, 249.
[85] L. Staudenmaier, *Ber. Deut. Chem. Ges.* **1898**, *31*, 1481.
[86] H. Hamdi, *Fortschrittsberichte über Kolloide und Polymere* **1943**, *54*, 554.
[87] J. William, S. Hummers, R. E. Offeman, *J. Am. Chem. Soc.* **1958**, *80*, 1339.
[88] S. Niyogi, E. Bekyarova, M. E. Itkis, J. L. McWilliams, M. A. Hamon, R. C. Haddon, *J. Am. Chem. Soc.* **2006**, *128*, 7720.
[89] M. Hirata, T. Gotou, S. Horiuchi, M. Fujiwara, M. Ohba, *Carbon* **2004**, *42*, 2929.
[90] N. I. Kovtyukhova, P. J. Ollivier, B. R. Martin, T. E. Mallouk, S. A. Chizhik, E. V. Buzaneva, A. D. Gorchinskiy, *Chem. Mater.* **1999**, *11*, 771.
[91] T. Nakajima, A. Mabuchi, R. Hagiwara, *Carbon* **1988**, *26*, 357.
[92] J. Lu, J.-x. Yang, J. Wang, A. Lim, S. Wang, K. P. Loh, *ACS Nano* **2009**, *3*, 2367.
[93] S. Stankovich, R. Piner, S. T. Nguyen, R. S. Ruoff, *Carbon* **2006**, *44*, 3342.
[94] A. Lerf, H. He, M. Forster, J. Klinowski, *J. Phys. Chem. B* **1998**, *102*, 4477.
[95] H. He, J. Klinowski, M. Forster, A. Lerf, *Chem. Phys. Lett.* **1998**, *287*, 53.
[96] L. J. Cote, F. Kim, J. Huang, *J. Am. Chem. Soc.* **2008**, *131*, 1043.
[97] D. Cai, M. Song, *J. Mater. Chem.* **2007**, *17*, 3678.
[98] J. I. Paredes, S. Villar-Rodil, A. Martínez-Alonso, J. M. D. Tascón, *Langmuir* **2008**, *24*, 10560.
[99] H. C. Schniepp, J. L. Li, M. J. McAllister, H. Sai, M. Herrera-Alonso, D. H. Adamson, R. K. Prud'homme, R. Car, D. A. Saville, I. A. Aksay, *J. Phys. Chem. B* **2006**, *110*, 8535.
[100] M. J. McAllister, J. L. Li, D. H. Adamson, H. C. Schniepp, A. A. Abdala, J. Liu, M. Herrera-Alonso, D. L. Milius, R. Car, R. K. Prud'homme, I. A. Aksay, *Chem. Mater.* **2007**, *19*, 4396.
[101] X. Sun, Z. Liu, K. Welsher, J. T. Robinson, A. Goodwin, S. Zaric, H. Dai, *Nano Res.* **2008**, *1*, 203.
[102] D. Li, M. B. Müller, S. Gilje, R. B. Kaner, G. G. Wallace, *Nat. Nanotechnol.* **2008**, *3*, 101.
[103] I. Jung, M. Vaupel, M. Pelton, R. Piner, D. A. Dikin, S. Stankovich, J. An, R. S. Ruoff, *J. Phys. Chem. C* **2008**, *112*, 8499.
[104] A. Buchsteiner, A. Lerf, J. Pieper, *J. Phys. Chem. B* **2006**, *110*, 22328.
[105] H.-K. Jeong, Y. P. Lee, M. H. Jin, E. S. Kim, J. J. Bae, Y. H. Lee, *Chem. Phys. Lett.* **2009**, *470*, 255.
[106] P. Blake, E. W. Hill, A. H. C. Neto, K. S. Novoselov, D. Jiang, R. Yang, T. J. Booth, A. K. Geim, *Appl. Phys. Lett.* **2007**, *91*, 063124.
[107] D. S. L. Abergel, A. Russell, V. I. Fal'ko, *Appl. Phys. Lett.* **2007**, *91*, 063125.
[108] I. Jung, M. Pelton, R. Piner, D. A. Dikin, S. Stankovich, S. Watcharotone, M. Hausner, R. S. Ruoff, *Nano Lett.* **2007**, *7*, 3569.
[109] E. Treossi, M. Melucci, A. Liscio, M. Gazzano, P. Samorì, V. Palermo, *J. Am. Chem. Soc.* **2009**, *131*, 15576.
[110] J. Kim, L. J. Cote, F. Kim, J. Huang, *J. Am. Chem. Soc.* **2009**, *132*, 260.
[111] L. Zhang, J. Liang, Y. Huang, Y. Ma, Y. Wang, Y. Chen, *Carbon* **2009**, *47*, 3365.
[112] C.-Y. Su, Y. Xu, W. Zhang, J. Zhao, X. Tang, C.-H. Tsai, L.-J. Li, *Chem. Mater.* **2009**, *21*, 5674.
[113] C. Gómez-Navarro, T. R. Weitz, A. M. Bittner, M. Scolari, A. Mews, M. Burghard, K. Kern, *Nano Lett.* **2007**, *7*, 3499.
[114] S. Gilje, S. Han, M. Wang, K. L. Wang, R. B. Kaner, *Nano Lett.* **2007**, *7*, 3394.
[115] V. C. Tung, M. J. Allen, Y. Yang, R. B. Kaner, *Nat. Nanotechnol.* **2009**, *4*, 25.
[116] A. B. Bourlinos, D. Gournis, D. Petridis, T. Szabo, A. Szeri, I. Dekany, *Langmuir* **2003**, *19*, 6050.
[117] Y. Si, E. T. Samulski, *Nano Lett.* **2008**, *8*, 1679.
[118] H.-J. Shin, K. K. Kim, A. Benayad, S.-M. Yoon, H. K. Park, I.-S. Jung, M. H. Jin, H.-K. Jeong, J. M. Kim, J.-Y. Choi, Y. H. Lee, *Adv. Funct. Mater* **2009**, *19*, 1987.
[119] J. Shen, Y. Hu, M. Shi, X. Lu, C. Qin, C. Li, M. Ye, *Chem. Mater.* **2009**, *21*, 3514.

[120] N. Mohanty, A. Nagaraja, J. Armesto, V. Berry, *Small* **2009**, *6*, 226.
[121] G. X. Wang, J. Yang, J. Park, X. L. Gou, B. Wang, H. Liu, J. Yao, *J. Phys. Chem. C* **2008**, *112*, 8192.
[122] Y. Chen, X. Zhang, P. Yu, Y. Ma, *Chem. Commun.* **2009**, 4527.
[123] X. Fan, W. Peng, Y. Li, X. Li, S. Wang, G. Zhang, F. Zhang, *Adv. Mater.* **2008**, *20*, 4490.
[124] Y. Zhou, Q. Bao, L. A. L. Tang, Y. Zhong, K. P. Loh, *Chem. Mater.* **2009**, *21*, 2950.
[125] E. Matuyama, *J. Phys. Chem.* **2002**, *58*, 215.
[126] X. Li, H. Wang, J. T. Robinson, H. Sanchez, G. Diankov, H. Dai, *J. Am. Chem. Soc.*, **2009**, *131*, 15939.
[127] V. Lee, L. Whittaker, C. Jaye, K. M. Baroudi, D. A. Fischer, S. Banerjee, *Chem. Mater.* **2009**, *21*, 3905.
[128] Z. Ming, W. Yuling, Z. Yueming, Z. Junfeng, R. Wen, W. Fuan, D. Shaojun, *Chem. Eur. J.* **2009**, *15*, 6116.
[129] G. K. Ramesha, S. Sampath, *J. Phys. Chem. C* **2009**, *113*, 7985.
[130] Z. Wang, X. Zhou, J. Zhang, F. Boey, H. Zhang, *J. Phys. Chem. C* **2009**, *113*, 14071.
[131] G. Williams, B. Seger, P. V. Kamat, *ACS Nano* **2008**, *2*, 1487.
[132] H. Ulrich, F. Alfred, *Ber. Dtsch. Chem. Ges.* **1930**, *63*, 1248.
[133] M. C. Kim, G. S. Hwang, R. S. Ruoff, *J. Chem. Phys.* **2009**, *131*, 064704.
[134] X. Gao, J. Jang, S. Nagase, *J. Phys. Chem. C* **2009**, *114*, 832.
[135] S. Gijie, S. Han, M. Wang, K. L. Wang, R. B. Kaner, *Nano Lett.* **2007**, *7*, 3394.
[136] H. Yamaguchi, G. Eda, C. Mattevi, H. Kim, M. Chhowalla, *ACS Nano* **2010**, *4*, 524.
[137] X. Li, G. Zhang, X. Bai, X. Sun, X. Wang, E. Wang, H. Dai, *Nat. Nanotechnol.* **2008**, *3*, 538.
[138] R. Y. N. Gengler, A. Veligura, A. Enotiadis, E. K. Diamanti, D. Gournis, C. Józsa, B. J. v. Wees, P. Rudolf, *Small 6*, 35.
[139] S. Park, J. An, J. W. Suk, R. S. Ruoff, *Small* **2009**, *6*, 210.
[140] L. Hu, D. S. Hecht, G. Gruner, *Nano Lett.* **2004**, *4*, 2513.
[141] Z. C. Wu, Z. H. Chen, X. Du, J. M. Logan, J. Sippel, M. Nikolou, K. Kamaras, J. R. Reynolds, D. B. Tanner, A. F. Hebard, A. G. Rinzler, *Science* **2004**, *305*, 1273.
[142] H. E. Unalan, G. Fanchini, A. Kanwal, A. Du Pasquier, M. Chhowalla, *Nano Lett.* **2006**, *6*, 677.
[143] G. Eda, Ph. D. Thesis, Rutgers University, New Brunswick, NJ, **2009**.
[144] Y. Zhou, Q. Bao, B. Varghese, L. A. L. Tang, C. K. Tan, C.-H. Sow, K. P. Loh, *Adv. Mater.* **2010**, *22*, 67.
[145] T. Szabó, O. Berkesi, P. Forgó, K. Josepovits, Y. Sanakis, D. Petridis, I. Dekány, *Chem. Mater.* **2006**, *18*, 2740.
[146] W. Cai, R. D. Piner, F. J. Stadermann, S. Park, M. A. Shaibat, Y. Ishii, D. Yang, A. Velamakanni, S. J. An, M. Stoller, J. An, D. Chen, R. S. Ruoff, *Science* **2008**, *321*, 1815.
[147] H. He, T. Riedl, A. Lerf, J. Klinowski, *J. Phys. Chem.* **1996**, *100*, 19954.
[148] A. Lerf, H. He, T. Riedl, M. Forster, J. Klinowski, *Solid State Ionics* **1997**, *101*, 857.
[149] C. Jian-Hao, W. G. Cullen, C. Jang, M. S. Fuhrer, E. D. Williams, *Phys. Rev. Lett.* **2009**, *102*, 236805.
[150] C. Hontoria-Lucas, A. J. López-Peinado, J. d. D. López-González, M. L. Rojas-Cervantes, R. M. Martín-Aranda, *Carbon* **1995**, *33*, 1585.
[151] T. Szabó, E. Tombácz, E. Illés, I. Dékány, *Carbon* **2006**, *44*, 537.
[152] T. Cassagneau, F. Guerin, J. H. Fendler, *Langmuir* **2000**, *16*, 7318.
[153] H.-K. Jeong, Y. P. Lee, R. J. W. E. Lahaye, M.-H. Park, K. H. An, I. J. Kim, C.-W. Yang, C. Y. Park, R. S. Ruoff, Y. H. Lee, *J. Am. Chem. Soc.* **2008**, *130*, 1362.
[154] D. W. Boukhvalov, M. I. Katsnelson, *J. Am. Chem. Soc.* **2008**, *130*, 10697.
[155] J. Robertson, E. P. O'Reilly, *Phys. Rev. B* **1987**, *35*, 2946.
[156] C. H. Lui, L. Liu, K. F. Mak, G. W. Flynn, T. F. Heinz, *Nature* **2009**, *462*, 339.
[157] E. Stolyarova, K. T. Rim, S. Ryu, J. Maultzsch, P. Kim, L. E. Brus, T. F. Heinz, M. S. Hybertsen, G. W. Flynn, *Proc. Natl. Acad. Sci.* **2007**, *104*, 9209–9212.
[158] K. A. Mkhoyan, A. W. Contryman, J. Silcox, D. A. Stewart, G. Eda, C. Mattevi, S. Miller, M. Chhowalla, *Nano Lett.* **2009**, *9*, 1058.
[159] K. N. Kudin, B. Ozbas, H. C. Schniepp, R. K. Prud'homme, I. A. Aksay, R. Car, *Nano Lett.* **2007**, *8*, 36.
[160] F. A. d. l. Cruz, J. M. Cowley, *Nature* **1962**, *196*, 468.
[161] F. A. d. l. Cruz, J. M. Cowley, *Acta Crystallogr.* **1963**, *16*, 531.
[162] N. R. Wilson, P. A. Pandey, R. Beanland, R. J. Young, I. A. Kinloch, L. Gong, Z. Liu, K. Suenaga, J. P. Rourke, S. J. York, J. Sloan, *ACS Nano* **2009**, *3*, 2547.
[163] J. I. Paredes, S. Villar-Rodil, P. Solís-Fernández, A. Martínez-Alonso, J. M. D. Tascón, *Langmuir* **2009**, *25*, 5957.
[164] D. Pandey, R. Reifenberger, R. Piner, *Surf. Sci.* **2008**, *62*, 1607.
[165] J.-L. Li, K. N. Kudin, M. J. McAllister, R. K. Prud'homme, I. A. Aksay, R. Car, *Phys. Rev. Lett.* **2006**, *96*, 176101.
[166] *CRC Handbook of Chemistry and Physics*, (Ed: D. R. Lide), Plenum, New York **2004**.
[167] A. C. Ferrari, J. Robertson, *Phys. Rev. B* **2000**, *61*, 14095.
[168] F. Tuinstra, J. L. Koenig, *J. Chem. Phys.* **1970**, *53*, 1126.
[169] A. C. Ferrari, J. C. Meyer, V. Scardaci, C. Casiraghi, M. Lazzeri, F. Mauri, S. Piscanec, D. Jiang, K. S. Novoselov, S. Roth, A. K. Geim, *Phys. Rev. Lett.* **2006**, *97*, 187401.
[170] A. Gupta, G. Chen, P. Joshi, S. Tadigadapa, P. C. Eklund, *Nano Lett.* **2006**, *6*, 2667.
[171] D. Graf, F. Molitor, K. Ensslin, C. Stampfer, A. Jungen, C. Hierold, L. Wirtz, *Nano Lett.* **2007**, *7*, 238.
[172] L. M. Malard, M. A. Pimenta, G. Dresselhaus, M. S. Dresselhaus, *Phys. Rep.* **2009**, *473*, 51.
[173] J. A. Robinson, M. Wetherington, J. L. Tedesco, P. M. Campbell, X. Weng, J. Stitt, M. A. Fanton, E. Frantz, D. Snyder, B. L. VanMil, G. G. Jernigan, R. L. Myers-Ward, C. R. Eddy, D. K. Gaskill, *Nano Lett.* **2009**, *9*, 2873.
[174] Z. Wei, D. E. Barlow, P. E. Sheehan, *Nano Lett.* **2008**, *8*, 3141.
[175] A. Das, S. Pisana, B. Chakraborty, S. Piscanec, S. K. Saha, U. V. Waghmare, K. S. Novoselov, H. R. Krishnamurthy, A. K. Geim, A. C. Ferrari, A. K. Sood, *Nat. Nanotechnol.* **2008**, *3*, 210.
[176] P. K. Ang, S. Wang, Q. Bao, J. T. L. Thong, K. P. Loh, *ACS Nano* **2009**, In press.
[177] V. Rakesh, D. Barun, R. Chandra Sekhar, C. N. R. Rao, *J. Phys.: Condens. Matter.* **2008**, *20*, 472204.
[178] M. A. Pimenta, G. Dresselhaus, M. S. Dresselhaus, L. G. Cançado, A. Jorio, R. Saito, *Phys. Chem. Chem. Phys.* **2007**, *9*, 1276.
[179] D. Yang, A. Velamakanni, G. Bozoklu, S. Park, M. Stoller, R. D. Piner, S. Stankovich, I. Jung, D. A. Field, C. A. Ventrice, Jr, R. S. Ruoff, *Carbon* **2009**, *47*, 145.
[180] A. C. Ferrari, J. Robertson, *Philos. Trans. R. Soc. A* **2004**, *362*, 2477.
[181] G. D. M. A. Pimenta, M. S. Dresselhaus, L. G. Cançado, A. Jorio, R. Saito, *Phys. Chem. Chem. Phys.* **2007**, *9*, 1276.
[182] M. Chhowalla, A. C. Ferrari, J. Robertson, G. A. J. Amaratunga, *Appl. Phys. Lett.* **2000**, *76*, 1419.
[183] S. Wang, P. K. Ang, Z. Wang, A. L. L. Tang, J. T. L. Thong, K. P. Loh, *Nano Lett.* **2010**, *10*, 92.
[184] H. Wang, J. T. Robinson, X. Li, H. Dai, *J. Am. Chem. Soc.* **2009**, *131*, 9910.
[185] V. López, R. S. Sundaram, C. Gómez-Navarro, D. Olea, M. Burghard, J. Gómez-Herrero, F. Zamora, K. Kern, *Adv. Mater.* **2009**, *21*, 1.
[186] I. Jung, D. A. Dikin, R. D. Piner, R. S. Ruoff, *Nano Lett.* **2008**, *8*, 4283.
[187] R. Saito, G. Dresselhaus, M. S. Dresselhaus, *Physical Properties of Carbon Nanotubes*, Imperial College Press, London **1998**.
[188] B. Partoens, F. M. Peeters, *Phys. Rev. B* **2006**, *74*, 075404.
[189] A. H. C. Neto, F. Guinea, N. M. R. Peres, K. S. Novoselov, A. K. Geim, *Rev. Mod. Phys.* **2009**, *81*, 109.
[190] J. Robertson, *Mater. Sci. Eng. R* **2002**, *37*, 129.
[191] M. F. Islam, E. Rojas, D. M. Bergey, A. T. Johnson, A. G. Yodh, *Nano Lett.* **2003**, *3*, 269.
[192] G. Eda, Y.-Y. Lin, C. Mattevi, H. Yamaguchi, H.-A. Chen, I.-S. Chen, C.-W. Chen, M. Chhowalla, *Adv. Mater.* **2009**, *21*, 505.

[193] Z. Luo, P. M. Vora, E. J. Mele, A. T. C. Johnson, J. M. Kikkawa, *Appl. Phys. Lett.* **2009**, *94*, 111909.
[194] Z. Liu, J. T. Robinson, X. Sun, H. Dai, *J. Am. Chem. Soc.* **2008**, *130*, 10876.
[195] D. Pan, J. Zhang, Z. Li, M. Wu, *Adv. Mater.* **2010**, *22*, 734.
[196] H. K. Jeong, M. H. Jin, K. P. So, S. C. Lim, Y. H. Lee, *J. Phys. D: Appl. Phys.* **2009**, *42*, 065418.
[197] R. J. W. E. Lahaye, H. K. Jeong, C. Y. Park, Y. H. Lee, *Phys. Rev. B* **2009**, *79*, 125435.
[198] J.-A. Yan, L. Xian, M. Y. Chou, *Phys. Rev. Lett.* **2009**, *103*, 086802.
[199] M. J. O'Connell, S. M. Bachilo, C. B. Huffman, V. C. Moore, M. S. Strano, E. H. Haroz, K. L. Rialon, P. J. Boul, W. H. Noon, C. Kittrell, J. Ma, R. H. Hauge, R. B. Weisman, R. E. Smalley, *Science* **2002**, *297*, 593.
[200] T. Gokus, R. R. Nair, A. Bonetti, M. Böhmler, A. Lombardo, K. S. Novoselov, A. K. Geim, A. C. Ferrari, A. Hartschuh, *ACS Nano* **2009**, *3*, 3963.
[201] J. Meihua, J. Hae-Kyung, Y. Woo Jong, B. Dong Jae, K. Bo Ram, L. Young Hee, *J. Phys. D: Appl. Phys.* **2009**, *42*, 135109.
[202] R. O. Grisdale, *J. Appl. Phys.* **1953**, *24*, 1288.
[203] D. T. Morrelli, C. Uher, *Phys. Rev. B* **1984**, *30*, 1080.
[204] S. Donner, H.-W. Li, E. S. Yeung, M. D. Porter, *Anal. Chem.* **2006**, *78*, 2816.
[205] P. Blake, P. D. Brimicombe, R. R. Nair, T. J. Booth, D. Jiang, F. Schedin, L. A. Ponomarenko, S. V. Morozov, H. F. Gleeson, E. W. Hill, A. K. Geim, K. S. Novoselov, *Nano Lett.* **2008**, *8*, 1704.
[206] A. Chipman, *Nature* **2007**, *449*, 131.
[207] J. Li, L. Hu, L. Wang, Y. Zhou, G. Gruner, T. J. Marks, *Nano Lett.* **2006**, *6*, 2472.
[208] J.-Y. Lee, S. T. Connor, Y. Cui, P. Peumans, *Nano Lett.* **2008**, *8*, 689.
[209] V. C. Tung, L.-M. Chen, M. J. Allen, J. K. Wassei, K. Nelson, R. B. Kaner, Y. Yang, *Nano Lett.* **2009**, *9*, 1949.
[210] J. Wu, M. Agrawal, H. t. A. Becerril, Z. Bao, Z. Liu, Y. Chen, P. Peumans, *ACS Nano* **2010**, *4*, 43.
[211] R. Czerw, B. Foley, D. Tekleab, A. Rubio, P. M. Ajayan, D. L. Carroll, *Phys. Rev. B* **2002**, *66*, 033408.
[212] Y. Park, V. Choong, Y. Gao, B. R. Hsieh, C. W. Tang, *Appl. Phys. Lett.* **1996**, *68*, 2699.
[213] G. Dennler, M. C. Scharber, C. J. Brabec, *Adv. Mater.* **2009**, *21*, 1323.
[214] Y.-M. Lin, K. A. Jenkins, A. Valdes-Garcia, J. P. Small, D. B. Farmer, P. Avouris, *Nano Lett.* **2008**, *9*, 422.
[215] Y. Zhang, J. P. Small, W. V. Pontius, P. Kim, *Appl. Phys. Lett.* **2005**, *86*, 073104.
[216] Y. Sui, J. Appenzeller, *Nano Lett.* **2009**, *9*, 2973.
[217] G. Eda, C. Mattevi, H. Yamaguchi, H. Kim, M. Chhowalla, *J. Phys. Chem. C* **2009**, *113*, 15768.
[218] J. Appenzeller, J. Knoch, V. Derycke, R. Martel, S. Wind, P. Avouris, *Phys. Rev. Lett.* **2002**, *89*, 126801.
[219] S. Heinze, J. Tersoff, R. Martel, V. Derycke, J. Appenzeller, P. Avouris, *Phys. Rev. Lett.* **2002**, *89*, 106801.
[220] V. M. Pereira, J. M. B. Lopes dos Santos, A. H. Castro Neto, *Phys. Rev. B* **2008**, *77*, 115109.
[221] S. Wang, P.-J. Chia, L.-L. Chua, L.-H. Zhao, R.-Q. Png, S. Sivaramakrishnan, M. Zhou, R. G. S. Goh, R. H. Friend, A. T. S. Wee, P. K. H. Ho, *Adv. Mater.* **2008**, *20*, 3440.
[222] J.-H. Chen, C. Jang, S. Xiao, M. Ishigami, M. S. Fuhrer, *Nat. Nanotechnol.* **2008**, *3*, 206.
[223] J.-H. Chen, C. Jang, S. Adam, M. S. Fuhrer, E. D. Williams, M. Ishigami, *Nature Phys.* **2008**, *4*, 378.
[224] B. Huard, N. Stander, J. A. Sulpizio, D. Goldhaber-Gordon, *Phys. Rev. B* **2008**, *78*, 121402.
[225] X. Wu, M. Sprinkle, X. Li, F. Ming, C. Berger, W. A. de Heer, *Phys. Rev. Lett.* **2008**, *101*, 026801.
[226] Z. Luo, Y. Lu, L. A. Somers, A. T. C. Johnson, *J. Am. Chem. Soc.* **2009**, *131*, 898.
[227] A. B. Kaiser, C. Gómez-Navarro, R. S. Sundaram, M. Burghard, K. Kern, *Nano Lett.* **2009**, *9*, 1787.
[228] N. F. Mott, E. A. Davis, *Electronic Processes in Non-Crystalline Materials*, Clarendon Press, Oxford **1979**.
[229] V. M. Pereira, J. M. B. L. d. Santos, A. H. C. Neto, *Phys. Rev. B* **2008**, *77*, 115109.
[230] L.-L. Chua, S. Wang, P.-J. Chia, L. Chen, L.-H. Zhao, W. Chen, A. T.-S. Wee, P. K.-H. Ho, *J. Chem. Phys.* **2008**, *129*, 114702.
[231] I. Jung, D. Dikin, S. Park, W. Cai, S. L. Mielke, R. S. Ruoff, *J. Phys. Chem. C* **2008**, *112*, 20264.
[232] G. E. Pike, C. H. Seager, *Phys. Rev. B* **1974**, *10*, 1421.
[233] X. Dong, D. Fu, W. Fang, Y. Shi, P. Chen, L.-J. Li, *Small* **2009**, *5*, 1422.
[234] M. Kaempgen, M. Lebert, M. Haluska, N. Nicoloso, S. Roth, *Adv. Mater.* **2008**, *20*, 616.
[235] I. Gierz, C. Riedl, U. Starke, C. R. Ast, K. Kern, *Nano Lett.* **2008**, *8*, 4603.
[236] H. Yang, C. Shan, F. Li, D. Han, Q. Zhang, L. Niu, *Chem. Commun.* **2009**, 3880.
[237] Y. W. Tan, Y. Zhang, K. Bolotin, Y. Zhao, S. Adam, E. H. Hwang, S. Das Sarma, H. L. Stormer, P. Kim, *Phys. Rev. Lett.* **2007**, *99*, 246803.
[238] P. G. Collins, K. Bradley, M. Ishigami, A. Zett, *Science* **2000**, *287*, 1801.
[239] B. B. Parekh, G. Fanchini, G. Eda, M. Chhowalla, *Appl. Phys. Lett.* **2007**, *90*, 121913.
[240] U. Dettlaff-Weglikowska, V. Skakalova, R. Graupner, S. H. Jhang, B. H. Kim, H. J. Lee, L. Ley, Y. W. Park, S. Berber, D. Tomanek, S. Roth, *J. Am. Chem. Soc.* **2005**, *127*, 5125.
[241] C. Klinke, J. Chen, A. Afzali, P. Avouris, *Nano Lett.* **2005**, *5*, 555.
[242] M. Terrones, P. M. Ajayan, F. Banhart, X. Blase, D. L. Carroll, J. C. Charlier, R. Czerw, B. Foley, N. Grobert, R. Kamalakaran, P. Kohler-Redlich, M. Rühle, T. Seeger, H. Terrones, *Appl. Phys. A* **2002**, *74*, 355.
[243] J. A. Robinson, E. S. Snow, S. C. Badescu, T. L. Reinecke, F. K. Perkins, *Nano Lett.* **2006**, *6*, 1747.
[244] Y.-M. Lin, P. Avouris, *Nano Lett.* **2008**, *8*, 2119.
[245] R. Verdejo, F. Barroso-Bujans, M. A. Rodriguez-Perez, J. A. d. Saja, M. A. Lopez-Manchado, *J. Mater. Chem.* **2008**, *18*, 2221.
[246] A. Yu, P. Ramesh, M. E. Itkis, E. Bekyarova, R. C. Haddon, *J. Phys. Chem. C* **2007**, *111*, 7565.
[247] J. Liang, Y. Huang, L. Zhang, Y. Wang, Y. Ma, T. Guo, Y. Chen, *Adv. Funct. Mater.* **2009**, *19*, 2297.
[248] T. Ramanathan, A. A. Abdala, S. Stankovich, D. A. Dikin, M. Herrera-Alonso, R. D. Piner, D. H. Adamson, H. C. Schniepp, X. Chen, R. S. Ruoff, S. T. Nguyen, I. A. Aksay, R. K. Prud'Homme, L. C. Brinson, *Nat. Nanotechnol.* **2008**, *3*, 327.
[249] S. Villar-Rodil, J. I. Paredes, A. Martínez-Alonso, J. M. D. Tascón, *J. Mater. Chem.* **2008**, *19*, 3591.
[250] S. Bajic, R. V. Latham, *J. Phys. D: Appl. Phys.* **1988**, *21*, 200.
[251] A. P. Burden, H. E. Bishop, M. Brierley, J. M. Friday, C. Hood, P. G. A. Jones, A. Y. Kyazov, W. Lee, R. J. Riggs, V. L. Shaw, R. A. Tuck, *J. Vac. Sci. Technol. B* **2000**, *18*, 900.
[252] S. Watcharotone, R. S. Ruoff, F. H. Read, *Phys. Procedia* **2008**, *1*, 71.
[253] R. H. Fowler, L. Nordheim, *Proc. R. Soc. Lond. A* **1928**, *119*, 173.
[254] Q. H. Wang, T. D. Corrigan, J. Y. Dai, R. P. H. Chang, A. R. Krauss, *Appl. Phys. Lett.* **1997**, *70*, 3308.
[255] K. Okano, S. Koizumi, S. R. P. Silva, G. A. J. Amaratunga, *Nature* **1996**, *381*, 140.
[256] I. Musa, D. A. I. Munindrasdasa, G. A. J. Amaratunga, W. Eccleston, *Nature* **1998**, *395*, 362.
[257] R. C. Smith, J. D. Carey, R. J. Murphy, W. J. Blau, J. N. Coleman, S. R. P. Silva, *Appl. Phys. Lett.* **2005**, *87*, 263105.
[258] E. Kymakis, G. A. J. Amaratunga, *Appl. Phys. Lett.* **2002**, *80*, 112.
[259] P. A. v. Hal, M. M. Wienk, J. M. Kroon, W. J. H. Verhees, L. H. Slooff, W. J. H. v. Gennip, P. Jonkheijm, R. A. J. Janssen, *Adv. Mater.* **2003**, *15*, 118.
[260] W. J. E. Beek, M. M. Wienk, M. Kemerink, X. Yang, R. A. J. Janssen, *J. Phys. Chem. C* **2005**, *109*, 9505.
[261] J. A. Rogers, *Nat. Nanotechnol.* **2008**, *3*, 254.
[262] B. Z. Jang, A. Zhamu, *J. Mater. Sci.* **2008**, *43*, 5092.

[263] Y. Xu, Y. Wang, J. Liang, Y. Huang, Y. Ma, X. Wan, Y. Chen, *Nano Res.* **2009**, *2*, 343.
[264] J. Liang, Y. Xu, Y. Huang, L. Zhang, Y. Wang, Y. Ma, F. Li, T. Guo, Y. Chen, *J. Phys. Chem. C* **2009**, *113*, 9921.
[265] R. Pasricha, S. Gupta, A. K. Srivastava, *Small* **2009**, *5*, 2253.
[266] G. Lu, S. Mao, S. Park, R. S. Ruoff, J. Chen, *Nano Res.* **2009**, *2*, 192.
[267] R. Muszynski, B. Seger, P. V. Kamat, *J. Phys. Chem. C* **2008**, *112*, 5263.
[268] C. Xu, X. Wang, J. Zhu, *J. Phys. Chem. C* **2008**, *112*, 19841.
[269] R. S. Sundaram, C. Gómez-Navarro, K. Balasubramanian, M. Burghard, K. Kern, *Adv. Mater.* **2008**, *20*, 3050.
[270] X. Zhou, X. Huang, X. Qi, S. Wu, C. Xue, F. Y. C. Boey, Q. Yan, P. Chen, H. Zhang, *J. Phys. Chem. C* **2009**, *113*, 10842.